Engineering Structures 276 (2023) 115308

Contents lists available at ScienceDirect

Engineering Structures

journal homepage: www.elsevier.com/locate/engstruct

# Experimental study of passive seismic vibration isolation by trench-type periodic barrier

Nagesh Ramaswamy [a], Bhagirath Joshi [b], Jiaji Wang [c,*], Xiaoliang Li [d], F.Y. Menq [e], Xiaonan Shan [f], Kalyana Babu Nakshatrala [g], K.H. Stokoe [h], Y.L. Mo [i]

[a] Department of Civil and Environmental Engineering, University of Houston, Houston, TX, USA
[b] Department of Civil and Environmental Engineering, University of Houston, Houston, TX, USA
[c] Department of Civil Engineering, the University of Hong Kong, Hong Kong, China
[d] Department of Electrical and Computer Engineering, University of Houston, Houston, TX, USA
[e] The University of Texas at Austin, Austin, TX, USA
[f] Department of Electrical and Computer Engineering, University of Houston, Houston, TX, USA
[g] Department of Civil and Environmental Engineering, University of Houston, Houston, TX, USA
[h] The University of Texas at Austin, Austin, TX, USA
[i] Department of Civil and Environmental Engineering, University of Houston, Houston, TX, USA

ARTICLE INFO

*Keywords:*
Periodic barrier
*T*-rex shaker
Excitation frequency
Excitation direction
Frequency response function
Frequency band gap

ABSTRACT

Seismic isolation systems protect structures and act as decoupling systems with the structure, which aims to uncouple the motion of the structure from incoming waves by reducing the kinetic energy of vibration transferred to structures. This research aims to study a non-invasive vibration isolation system using periodic barriers. A comprehensive field test program is completed to evaluate the wave isolation performance of empty trench and periodic barriers. The precast one-dimensional (1D) periodic barriers are arranged to form one long barrier and one short thick barrier to examine the influence of barrier length and the number of unit cells on the vibration isolation performance. The test program reported in this study is the P0 case (without periodic foundation), which serves as a reference group compared to previous test case *P*1 (with periodic barrier and reinforced concrete foundation) and test case *P*2 (with a combination of periodic barrier and periodic foundation). The triaxial (*T*-Rex) shaker truck generates excitation in three axis and the wave form include sine wave, sweep frequency and seismic waves. Each geophone sensor position records the triaxial soil response. The responses of soil along the direction of wave transfer, the normalized responses, and the frequency response function (FRF) are all provided and discussed. Various excitation inputs are comparable. It is found that the excitation directions influence the periodic barrier's effectiveness because of the dominant waveform. When FRF is compared between benchmark case and test cases, the periodic barriers' screening effectiveness can be determined in the attenuation zones. These attenuation zones are expected to be the frequency band gaps of the periodic barrier. When the incoming wave frequency falls in this frequency band gap, the periodic barrier can isolate the vibration propagating towards the protected region.

## 1. Introduction

A non-invasive periodic barrier is a combination of a trench and a 1D periodic barrier. The advanced seismic isolation performance of the periodic barrier is developed based on the selective vibration isolation property of the existing periodic foundation [1–6]. The periodic barrier is expected to provide both advantages of wave barrier and periodic material when infilled in trench type barrier. The periodic barrier is installed away from the structure, acting as a non-invasive vibration isolation system. The disadvantages of the periodic foundation are overcome with this trench-type periodic barrier since it is easy to be installed and maintained. It does not need to carry the superstructure

* Corresponding author.
*E-mail addresses:* nhoraked@cougarnet.uh.edu (N. Ramaswamy), bjoshi2@central.uh.edu (B. Joshi), cewang@hku.hk (J. Wang), xli67@cougarnet.uh.edu (X. Li), fymenq@utexas.edu (F.Y. Menq), xshan@central.uh.edu (X. Shan), knakshatrala@uh.edu (K. Babu Nakshatrala), k.stokoe@mail.utexas.edu (K.H. Stokoe), yilungmo@central.uh.edu (Y.L. Mo).

https://doi.org/10.1016/j.engstruct.2022.115308

Available online 9 December 2022

load since it is independent of the structure. The proposed trench-type periodic barrier will add immense value to seismic isolation systems and the field of earthquake engineering.

Wave barriers are a typical type of vibration isolation system to prevent structures from seismic vibrations. The damages due to seismic vibrations and human-induced vibrations to structures led researchers to study and develop measures to isolate the vibrations reaching the structure. Wave barriers are developed to isolate the vibrations by creating a discontinuity in the wave propagation path. To protect structures from seismic vibrations, they are often installed underground. Different forms of wave barriers are developed, such as open or infilled trench-type wave barriers [7–15] and rows of piles [16–20]. Typically wave barriers are in the form of open or infilled trench types. Even though studies found that open trenches show higher wave isolation performance compared to infilled trenches, the instability of the soil makes the open trenches hard to maintain and sometimes becomes an unsafe condition for people's safety, so the various infilled materials are investigated in this study. Based on the distance between the excitation source and the barrier, they are classified as either active or passive isolation wave barriers. When the barrier is installed in the vicinity of the vibration source to isolate the vibration, it is called an active isolation wave barrier. These are usually used when the source of vibration is known. When the barrier is installed close to the structure to isolate the vibration, it is called a passive isolation wave barrier [2]. Based on infilled material, for soft barriers, Young's modulus and shear modulus of infilled material are smaller than those of soil; for the stiff barrier, Young's modulus and shear modulus of infilled material are greater than those of soil.

A periodic material is a non-natural material designed with an assembly of different composite materials to exhibit negative refractive index property and have selective frequency band gaps [6,21–25]. It is also called metamaterial, and the concept originates based on the selective frequency band gap property of phononic crystals from solid-state physics. Phononic crystals can control the wave propagation in a select frequency range. When these phononic crystals are used in a large scale, it is called periodic structure. The materials are usually arranged in repeating patterns at smaller scales than the wavelengths of the phenomena they influence. An adequately designed metamaterial can manipulate incoming waves by blocking or reflecting them to provide benefit, which is not possible with conventional materials [1].

Many researches have been done in past decades to evaluate the vibration isolation by periodic barrier. A large-scale field experiment in a marble quarry was conducted by Meseguer et al., [23]. A collection of periodically distributed cylindrical holes were drilled on the marble surface. Surface elastic waves were generated up to 40 kHz using 0.5 in steel bearing ball in two directions. One is in line with response detectors, and the other is inclined at 30 degrees to sensors. The results showed that wave attenuation zones exist in both cases. The conclusion was made on the existence of attenuation zones for Rayleigh waves by periodically distributed cylindrical holes. An acoustic barrier adapting the periodic material was tested in the outdoor environment with frequencies between 500 and 4000 Hz by Sanchez-Perez et al., [26]. This acoustic barrier is formed by two-dimensional arrays of hollow cylinders in air. The microphone and the source were placed in several positions to analyze the transmission sound from a different direction. The test concluded that the attenuation zone could be adjusted by varying the constant lattice and the filling fraction, and a limited number of elements can attain the attenuation level achieved by other acoustic screens. The work also proves the periodic material can reduce noise not only in controlled condition such as an echo-free chamber but also in free-field conditions with the insertion loss higher than 11 dB within the frequency band gap. The acoustic band gap associated with periodic elastic composite were also validated analytically by Kushwaha et al. 1993 [27]. Yan et al. 2014 [28] reported the basic theory of 2D periodic foundation to prevent the structure from seismic vibration. A FEM for 2D periodic foundation with a superstructure was setup to evaluate the frequency band gap by frequency analysis. Small-scale experimental results were compared with FEM results for conclusive study. The results confirm the significant vibration attenuation when the exciting frequency falls into the band gaps and coincide with both theoretical and experimental results. Extensive numerical studies have been made by many researchers to evaluate the vibration isolation performance and existence of frequency band gap [2,5,6,20,29,30].

The design of a 1D layered periodic barrier was presented by Witarto et al. [1] which is based on selective frequency isolation by Phononic crystals [21,31]. The crystal lattice arranged in one direction possesses frequency isolation when the propagation is normal to the direction of the lattice. Various dimension 1D unit cell periodic structures and the variation of frequency band gap with respect to the width of unit cell, thickness ratio, and effect of Young's modulus and Poisson's ratio were studied. The frequency band gap of benchmark unit cell periodic structure consisting of one concrete base and one rubber layer was found to be 13.51 Hz– 30.87 Hz and 36.65 Hz to 50 Hz for S-waves, and the frequency band gap for P-waves was found to be between 51.5 Hz and 117.6 Hz. A simple unit cell 1D periodic barrier consisting of a rubber layer sandwiched between concrete layers with different thickness ratios was studied to analyze the effect of Young's modulus and Poisson's ratio. The effects of Young's modulus and Poisson's ratio were not much significant. The conclusion was made that the unit cell must consist of at least two contrasting components, i.e., stiff, and dense components as well as light and soft components. More number of unit cells provides better wave attenuation. Large plane size to the total thickness of periodic structure can eliminate undesirable vibrations. Xiang et al. [32] conducted shake table tests on a specimen with periodic foundation and without periodic foundation to evaluate the response reduction efficiency of periodic foundation for transverse and longitudinal waves and compared it with numerical analysis results. Similar performance evaluation experiments and numerical analysis were conducted by Zhao et al. 2021 [3] on a small modular reactor with a 1D periodic foundation. The results show the existence of frequency band gaps, and when the frequency of incoming wave falls in the band gap, the periodic foundation can isolate the vibration to protect the superstructure from seismic damage. Witarto et al. [33] presented the global sensitivity analysis of frequency band gap in 1D Phononic crystals based on the variance decomposition and material parameters using a mathematical model with respect to input parameters. The width of the frequency band is dependent on the interaction of thickness ratio and Young's modulus for S-waves. For P-Waves, the Poisson's ratio interaction of the reference layer is an additional dominating parameter.

The goal of the research is fourfold: (1) test and evaluate the attenuation zones of periodic barrier experimentally and compare with the theoretical frequency band gap, (2) conduct a series of passive isolation tests to evaluate the vibration isolation by the periodic barrier, (3) develop a periodic barrier setup which can provide total isolation of vibration by conducting large-scale field experiments and (4) check the feasibility for seismic vibration isolation. The condition with periodic barrier and empty trench is also included in the scope of the study. The test condition without a barrier serves as the benchmark case to evaluate the vibration isolation by the barrier. The empty trench case results provide a significant comparison with the material-infilled cases. The vibration isolation by the periodic barrier is validated experimentally in this study. The influence of critical parameters such as excitation direction and distance on the vibration isolation performance and frequency band gaps is critically examined.

## 2. Theory of 1D periodic materials

Periodic materials exhibit selective frequency band gap property. These frequency band gaps can be obtained by constructing dispersion curves of a unit cell periodic material by applying periodic boundary conditions. Many researchers contributed to the theoretical study of periodic materials to obtain dispersion curves and to derive theoretical

frequency band gaps. Some of those methods include transfer matrix method [1,2,3,4,39,41,42]. The derivation of frequency band gap of metamaterial using transfer matrix method for P wave and S wave was described by Witarto et al. [1,4,39], Zhao et al. [3] and for Rayleigh wave was described by Huang [2]. By solving wave equation for P wave, S wave, and Rayleigh wave and by applying periodic boundary conditions to top and bottom surface of periodic material, the relationship between wavenumber and frequency can be obtained. Eqs. (1), (2), and (3) show the wave equations for homogeneous materials of the P wave, S wave, and Rayleigh wave, respectively as follows:

$$\frac{\partial^2 u}{\partial t^2} = C_P^2 \frac{\partial^2 u}{\partial x^2} \ , \tag{1}$$

$$\frac{\partial^2 w}{\partial t^2} = C_S^2 \frac{\partial^2 w}{\partial x^2} \ , \tag{2}$$

$$\begin{cases} \dfrac{\partial^2 \phi}{\partial t^2} = C_P^2 \left( \dfrac{\partial^2 \phi}{\partial x^2} + \dfrac{\partial^2 \phi}{\partial z^2} \right) = C_P^2 \left( \dfrac{\partial u}{\partial x} + \dfrac{\partial w}{\partial z} \right) \\ \dfrac{\partial^2 \psi}{\partial t^2} = C_S^2 \left( \dfrac{\partial^2 \psi}{\partial z^2} + \dfrac{\partial^2 \psi}{\partial x^2} \right) = C_S^2 \left( \dfrac{\partial u}{\partial z} - \dfrac{\partial w}{\partial x} \right) \end{cases} , \tag{3}$$

where $u$ denotes the $x$-direction displacement, $w$ denotes the z-direction displacement, $C_S$ denotes S wave velocity, $C_P$ denotes the P wave velocity. $\phi$ and $\psi$ are dilatational potential and rotational potential, respectively. By substituting these wave equations into steady state oscillatory wave equations, the general solution to $n^{th}$ layer can be obtained [1,2,3,4,39].

The resulting state vector for $n^{th}$ layer is further reduced to eigenvalue problem by using transfer matrix and Bloch-Floquent theory as in Eq. (4)

$$\left| \boldsymbol{T}(\omega) - e^{ika} \boldsymbol{I} \right| = 0. \tag{4}$$

where $e^{ika}$ is the Eigenvalue of the transformation matrix $\boldsymbol{T}(\omega)$. By solving the Eigenvalue problem, the relationship between wavenumber $k$ and frequency $\omega$ can be obtained. To obtain the frequency band gaps, wave number $k$ is considered only limited to Brillouin zone [38], i.e., $k \in [-\pi/h, \pi/h]$ even though $k$ is unrestricted.

Researchers also developed few other theoretical methods to obtain dispersion curve and derived frequency band gaps which include plane wave expansion (PWE) [27,43], finite difference time domain (FDTD) [44,45], finite element methods (FEM) [2,4].

## 3. Experimental program

### 3.1. Specimen specification

A 1D periodic barrier consisting of two reinforced concrete layers and one polyurethane layer is used in this study [34–36]. The design of this 3-layer unit cell and the properties of polyurethane are the same as reported by Witarto et al. [4]. The same batch of polyurethane layers is used in this experiment. Witarto developed the dispersion relation of periodic foundation and the obtained frequency band gaps within the range of 5 to 100 Hz. For the P wave, the theoretical frequency bandgap is 45.0–100 Hz; for the S wave, the theoretical frequency band gaps are 11.8–46.1 Hz, 49.1–92.1 Hz, and 93.7–100 Hz; for the Rayleigh wave, the frequency band gaps are 10.2–43.8 Hz, 47.0–87.6 Hz, and 88.8–100 Hz [29] The frequency band gaps are designed to stay below 100 Hz due to the earthquake engineering application and the limitation of the triaxial shaker (*T*-Rex) [37] used in this experiment.

The fabrication process of the specimen is as reported in Huang 2020 [2]. The overall dimensions of the 3-layer unit cell specimen are 1.52 ft long, 1.22 ft wide, and 0.28 ft thick, in which the first and third layer of reinforced concrete has the dimension of 1.52 ft long, 1.22 ft wide, and 0.1 ft thick. The 1D 3-layer unit cell specimen for the experimental field study is shown in Fig. 1.

### 3.2. Test setup

This experimental program consists of 4 passive isolation tests with different barrier conditions. Each test is distinct in terms of infilled material in the trench, periodic barrier dimension, and the number of periodic barriers. In this experiment, the different test conditions are classified as i) No Barrier (P0S0), ii) Empty long trench (P0EL), iii) Single long Barrier, and iv) One thick Barrier. The detailed description is shown in Fig. 2. Compared to previous research, this study presents the test results of periodic barrier without the influence of superstructure or periodic foundation. This test program serves as a reference group compared to previous research, which show a combination of periodic barrier, periodic foundation, and superstructure [34–36].

In the experimental program, the P0S0 condition is considered a benchmark case with a ground surface response without any trench and periodic barrier. Table 1 shows the dimensions of the barrier associated with the test condition.

Each test condition is subjected to three different excitation inputs i) frequency sweep excitation, ii) fix frequency harmonic excitation, and iii) earthquake excitation in all three directions individually, such as Vertical excitation direction, Horizontal crossline excitation direction, and Horizontal inline excitation direction to study the vibration isolation performance in different directions of excitation by measuring the response in the direction same as excitation. Frequency sweep excitation ranges from 15 Hz to 100 Hz with a predefined duration of 12 s, with preselected frequency cycles, the excitation produces one frequency at a time within the selected frequency range. This allows us to obtain and analyze the vibration isolation performance in a short duration of time. Fix frequency harmonic excitation is the signal with constant frequency and amplitude applied for a duration of 2 s. This frequency ranges from 15 Hz to 100 Hz with an increment of 5 Hz. Due to the concentrated energy of the applied frequency, this will have a high signal-to-noise ratio to obtain a better response. Lastly, earthquake excitations consisting of nine individual earthquake seismograms Oroville, Anza, Bishop, Loma Prieta, TCU052, Gilroy, San Fernando, El Centro, and Northridge are provided as input. These earthquakes' original time history data are obtained from the PEER ground motion database. Since the estimated frequency bandgap range is 10 Hz to 100 Hz, and the optimum performing range of frequency of *T*-Rex is 10 Hz to 100 Hz, these earthquake frequencies are scaled to maintain the frequency range between 10 Hz and 100 Hz by multiplying with the scale factor [34]. The Earthquake seismograms are used as the input excitation to *T*-Rex shaker. The excitation is applied in the three various directions in each test scenario to get the isolation performance of the periodic barrier in the same direction of excitation.

**Fig. 1.** A 1D 3-layer Unit Cell Periodic Barrier Specimen [2].

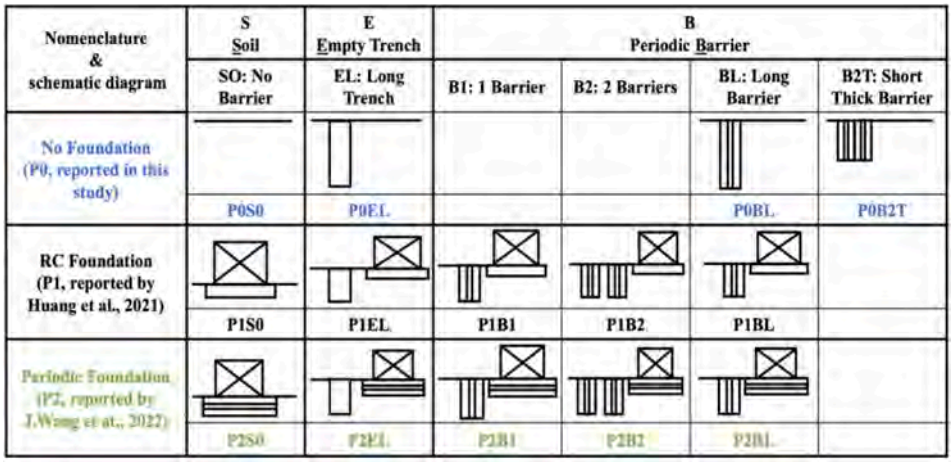


**Fig. 2.** Schematic Representation of Test Plan (not to scale) Note: Scenario P1 was reported by Huang et al. [34], scenario P2 and the comparison between scenario P1 and scenario P2 was reported by J. Wang et al. [36]. The *P*1 tests were completed in October 2019, P2 tests were completed in June 2020, P0 test scenarios were completed in April 2022.

**Table 1**
Barrier dimensions.

| Barrier condition | Description | Length (ft) | Depth (ft) | Width (ft) |
|---|---|---|---|---|
| EL | One long empty trench | 2.44 | 1.52 | 0.28 |
| BL | One long periodic barrier | 2.44 | 1.52 | 0.28 |
| B2T | One short thick periodic barrier | 1.22 | 1.52 | 0.56 |

A passive isolation test condition can be defined as placing the barrier away from the excitation source to absorb and isolate the frequency reaching the structure or region behind the barrier. The five various test conditions have a specific mapping of the sensor, accelerometer, and the location of the barrier to be followed during the field test. The distance of excitation source (*T*-Rex) from the periodic barrier is one parameter that distinguishes this experiment program into two different sets. When the distance between barrier and source is 20ft, it is termed as near field excitation; similarly, when the distance is 100ft, it is termed as far-field excitation—Fig. 3, Fig. 4, Fig. 5, and Fig. 6 show on-field sensor mapping.

A total of 45 geophones are placed, as shown in the sensor layout, to record the response in the three various directions. 15 geophones for Vertical excitation response, 15 for Horizontal Inline excitation response, and 15 for Horizontal crossline response. Each location will have three geophones, as shown in Fig. 7. The red color geophone records response in the vertical direction, and two blue geophones record responses in Horizontal inline and crossline directions. The geophones used in the tests are GS-One LF 4.5 Hz. The natural frequency of the geophone is 4.5 Hz, the calibration factor is 2.303 V/(in/*sec*), and the damping coefficient is 0.7.

The triaxial micro-electrical mechanical system accelerometers are fixed on both sides of the barrier, as shown in Fig. 8, to record response before and after the barrier. These accelerometers record responses to excitation in all three directions. X-direction refers to Horizontal inline direction, Y-direction refers to Vertical direction, and Z- direction refers to Horizontal inline direction. Silicon Design, Inc 2430–002 model accelerometers are used in the tests. The calibration factor is 2.5 V/g.

### 3.3. Site investigation

By conducting Spectral-Analysis-of-Surface-Waves (SASW) test we can determine the shear wave velocity profile of the test site [2]. By utilizing the dispersive nature of Rayleigh-type surface waves propagating through a layered material to determine the shear wave velocity profile of the material, this test method provides the dispersion curve of the soil profile. The surface waves are generated at one location on the ground surface and the vertical motions created by the passage of surface waves between the pairs of receivers are recorded using a dynamic signal analyzer to interpret the relative phase of the cross-power spectrum between the two receivers of each receiver pair. The data collected in the field in the form of phase plots, are reduced and interpreted, which provides the dispersion curve which represents relationship between the phase velocity and wavelength of the surface wave for the test site. The surface wave dispersion curve was measured, and the site's following shear wave velocity profile was obtained as shown in Fig. 9.

From Fig. 9, the shear wave velocity (V) of the first layer located between 0 and 0.625 m below ground surface is 90 m/*sec*, and the second layer located between 0.625 and 2.125 m below ground surface is 161.5 m/*sec*. The depth beyond 2.1 m is the third layer, and the associated shear wave velocity is 234.7 m/*sec*. The soil sample at each layer from the site is collected, and properties are measured in the laboratory. The first layer of 1ft depth below the ground surface has a density (ρ) of 1630 kg/m3, and the density at a depth of 3ft below the ground surface is 1702 kg/m3. The assumed Poisson ratio is 0.33 for

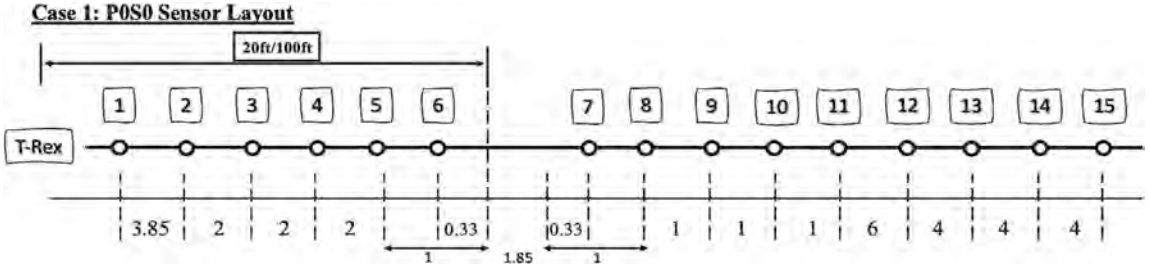


**Fig. 3.** Case 1: No Barrier (P0S0) Sensor Layout (in units of ft).

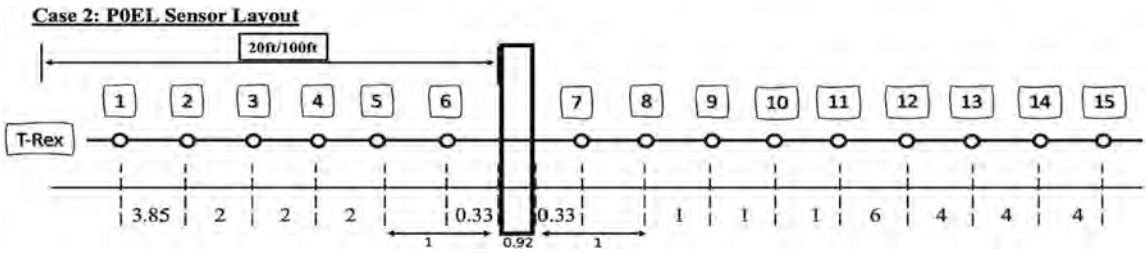


**Fig. 4.** Case 2: Long Empty Trench (P0EL) Sensor Layout (in units of ft).

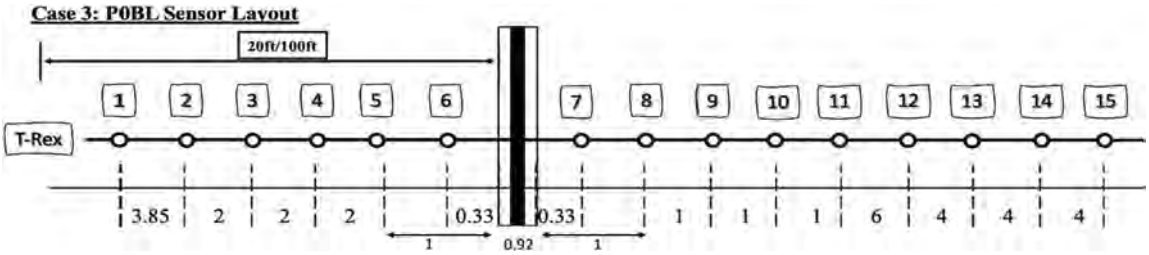


**Fig. 5.** Case 3: One Long Periodic Barrier (P0BL) Sensor Layout (in units of ft).

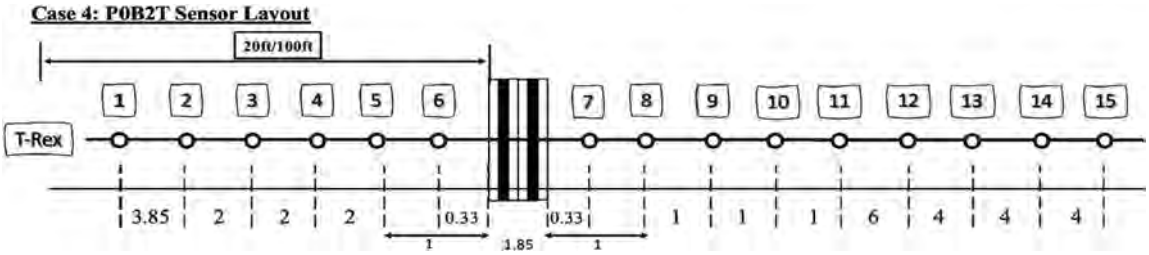


**Fig. 6.** Case 4: One Short Thick Periodic Barrier (P0B2T) Sensor Layout (in units of ft).

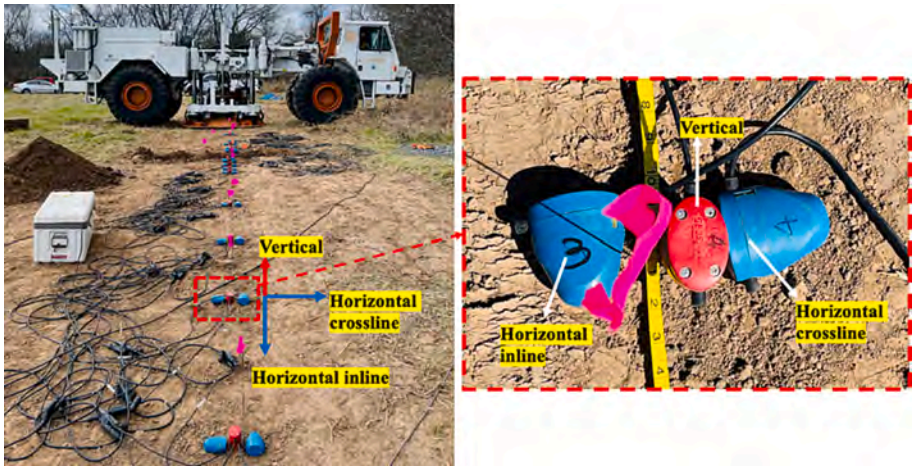


**Fig. 7.** 3D geophone directions.

unsaturated soil. The Young's modulus is calculated using.

Shear modulus,

$$G = \rho V^2 \tag{24}$$

and Young's modulus,

$$E = \frac{G}{(2(1+))} \tag{25}$$

Therefore, the calculated Young's modulus for the first, second, and third layers is 35 MPa, 118 MPa, and 249 MPa, respectively [2]. The data acquisition methodology involves a function generator, a data acquisition system (mobilizer), and an excel input sheet [2,34].

### 3.4. Data processing

The *T*-Rex shaker can produce dynamic vibration in all three directions. The input signals, i.e., frequency, duration, and sampling rate for the designated test are sent to the function generator using the excel

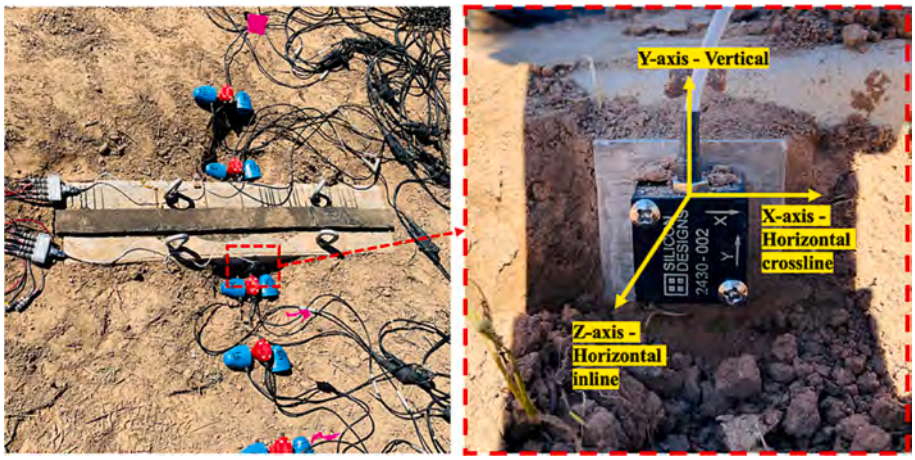


**Fig. 8.** 3D Accelerometer.

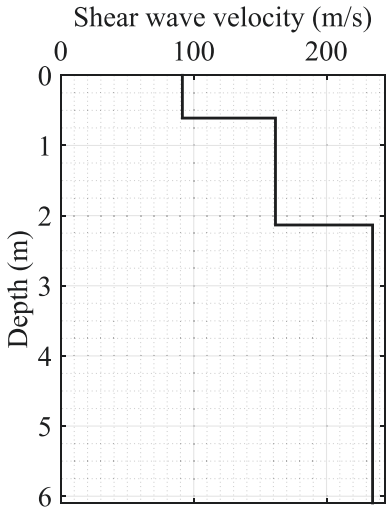


**Fig. 9.** Shear wave velocity profile obtained from SASW test [2].

sheet. The *T*-Rex input channel is connected to the function generator. By pressing the trigger button, the signal is sent to *T*-Rex. The *T*-Rex will generate the vibration in a preset direction. When the vibration passes through installed geophones, the geophones will record the response in Voltage. Also, the accelerometer records the response in Voltage. Each test run is saved.

The recorded data from the geophone might be more than the required duration of the test. To eliminate those recorded data outside test duration, the Tukey-window function, a cosine-tapered window function from MATLAB with cosine fraction 0.12, is used to make data outside test duration to zero. The natural frequency of geophone (4.5 Hz) and response beyond 100 Hz are eliminated by applying a fifth-order low-pass and high-pass Butterworth filter, an anti-aliasing function from MATLAB to attenuate the signal below 5 Hz and above 100 Hz by setting the low-pass cutoff frequency to 5 Hz and high-pass cutoff frequency to 100 Hz. Now, the data in velocity is converted to acceleration by taking the gradient of velocity with respect to time. The data is plotted as acceleration versus time to represent the response in the time domain. By applying Fast Fourier Transformation (FFT), we can obtain the response in the frequency domain as acceleration vs frequency.

The isolation performance of the periodic barrier is evaluated by calculating Frequency Response Function (FRF) and the response in the same direction as the excitation direction. There are different methods to calculate FRF. One such method is the Direct Method. The direct method uses the response at the nearest point before the barrier and the nearest point after the barrier to calculate FRF. Different test condition uses a different approach to process the data. The maximum acceleration can be obtained from the frequency domain for the fix-frequency harmonic excitation test. For fix-frequency harmonic excitation, the expression to calculate FRF using the direct method for each exciting frequency $f_i$ is

$$FRF_{f_i} = 20log_{10}\left[\frac{|A_{f_i}(t)|_{max,back}}{|A_{f_i(t)}|_{max,front}}\right] \tag{26}$$

where $|A_{f_i}(t)|_{max,back}$ is the absolute value of the maximum acceleration record at the nearest point behind barrier,

$|A_{f_i}(t)|_{max,front}$ is the absolute value of the maximum acceleration record at the nearest point in front of the barrier. For frequency sweep and earthquake excitation input, the expression to calculate FRF using the direct method is

$$FRF(f) = 20log_{10}\left[\frac{|A(f)|_{back}}{|A(f)|_{front}}\right] \tag{27}$$

where $|A(f)|_{back}$ is the response in the frequency domain at the nearest point behind the barrier,

$|A(f)|_{front}$ is the response in the frequency domain at the nearest point in front of the barrier.

The FRF is calculated for frequency domain data. The final FRF for earthquake excitation is obtained by averaging the FRF of nine earthquakes.

Using the direct method, the response at the point before the barrier and after the barrier can be directly compared without normalization. By comparing the FRF of each test case with the benchmark case, we can analyze the isolation performance of barriers. The vibration attenuation zone is identified when the FRF of with barrier case is smaller than in the case without the barrier. The vibration amplification zone is identified when the FRF of with barrier case is higher than in the case without the barriers.

## 4. Experimental results

The test results with various conditions are discussed in this section. The processed data is represented graphically in comparison to the benchmark case to analyze the isolation performance of various barrier conditions. The fix-frequency harmonic excitation test results are compared in two ways. One compares normalized acceleration versus distance from the excitation source for each frequency, and the other compares the FRF of each barrier case with the FRF of the benchmark case. The results of the frequency sweep and earthquake excitation are

compared using FRF with the benchmark case. The distance between the barrier and excitation source (*T*-Rex) is a key factor in the tests. The *T*-Rex is placed at two different distances of 20 ft and 100 ft from the periodic barrier. When *T*-Rex is placed at a 20 ft distance from the barrier, it is called near-field excitation. When the *T*-Rex is placed at a 100 ft distance from the barrier, it is called far-field excitation.

### 4.1. No barrier (P0S0)

The test condition with no barrier is considered a benchmark case denoted as P0S0. The sensor mapping is shown in Fig. 3. The *T*-Rex is placed at a 20 ft distance. The input signal is provided, and the responses of all sensors are recorded. The procedure is repeated for various excitation directions, and the responses are recorded. The *T*-Rex is moved to a 100 ft distance from the barrier, the input signal is provided, and the responses of all sensors are recorded. The procedure is repeated for various excitation directions. Following the data processing procedure as mentioned in Section 3.4 the following results are observed. Fig. 10 shows the maximum steady-state response recorded at various sensor locations in all three directions.

The *T*-Rex shaker does not provide exactly same vibration as input even though the input signal is the same and slight differences in magnitude may occur. The response comparison for various barrier conditions without normalizing the response will provide inappropriate results. Therefore, dividing the response by reference point will provide a normalized response. The reference point is located between the excitation source and the point nearest to the barrier, i.e., sensor 6 is taken as the reference point. The normalized response at the reference point is always one. Fig. 11 shows normalized responses of all sensors in the vertical direction for an excitation distance of 20ft with fix-frequency harmonic excitation at 15 Hz and 75 Hz.

The FRFs of the benchmark cases with the fix-frequency harmonic excitation, frequency sweep, and earthquake excitation are calculated using the direct method, as explained in Section 3.4, as references to evaluate the isolation performance of barriers. Fig. 12 shows the FRF of the P0S0 case in the vertical direction for an excitation distance of 20ft.

With these results from the benchmark case, we can compare various barrier conditions to evaluate the isolation performance of barriers.

### 4.2. Long empty trench (P0EL)

A long-empty trench of the length of 8 ft, depth of 5 ft, and width of 0.92 ft is located between sensors 6 and 7, as shown previously in sensor mapping. When a fix-frequency harmonic excitation is applied at a distance of 20 ft and 100 ft in all three directions, the ground surface responses are recorded in all three directions by the sensors. The critical points for observation are sensors 6 and 7. The normalized response is obtained by dividing the responses of sensors 6 to 15 by sensor 6, which is the nearest sensor before the long empty trench. When 15 Hz and 75 Hz harmonic excitations are applied at a distance of 20 ft from the barrier, the response reduction after the long empty trench is observed. Fig. 13 shows the normalized maximum response at the sensor locations after the barrier under a fix-frequency harmonic excitation at a distance of 20 ft from the barrier. The black curve represents the benchmark case (P0S0), and the red curve represents the long empty trench case (P0EL).

It is shown in Fig. 13 (b) that when a 15 Hz harmonic excitation is applied at a distance of 100 ft from the barrier, significant response reduction after the long empty trench is observed in the horizontal inline excitation direction. In contrast, the other two excitation directions do not give response reduction compared with the benchmark case, as shown in Fig. 13 (a) and Fig. 13 (c). When a 75 Hz harmonic excitation is applied at a distance of 100 ft from the barrier, significant response reduction after the long empty trench is observed in the vertical excitation direction, as shown in Fig. 13 (d). The other two directions do not give response reduction when compared with the benchmark case [Fig. 13 (e) and Fig. 13 (f)]. Fig. 14 shows the normalized maximum responses at sensor locations after the barrier under a fix-frequency harmonic excitation at a distance of 100 ft. The black curve represents the benchmark case (P0S0), and the red curve represents the long empty trench case (P0EL).

To evaluate the effect of excitation distance on the performance of the periodic barrier, the normalized response of the P0EL case is represented for fix-frequency harmonic excitation of 30 Hz at a distance of 20 ft (Black curve), and 100 ft (Red curve) under all three directions of excitation is represented in Fig. 15.

The normalized ground surface response can be larger when the excitation distance increases. This means less response reduction is realized when the excitation distance is larger, as shown in Fig. 15 (a)-(c). The ground surface response decays as the distance from the vibration source increases. The exponential decay suggests that the response reduction decreases drastically when the distance from the vibration source increases. The response reduction from one sensor location to the other becomes very small. Therefore, the normalized response is higher when the excitation distance is larger.

When the other two input signals, i.e., frequency sweep and earthquake excitation are applied, the responses are recorded by all the sensors. The two critical sensor locations are identified to evaluate the vibration isolation performance of the barrier. Sensor 6 is the nearest point before the barrier, and the response is considered as input to the barrier. Sensor 7 is the nearest point after the barrier, and the response is considered as output from the barrier. The results are represented in the frequency domain to evaluate the effect of exciting frequency on the barrier's performance. The ground surface response from the P0S0 case is represented in Fig. 16, which shows the characteristics of the test site.

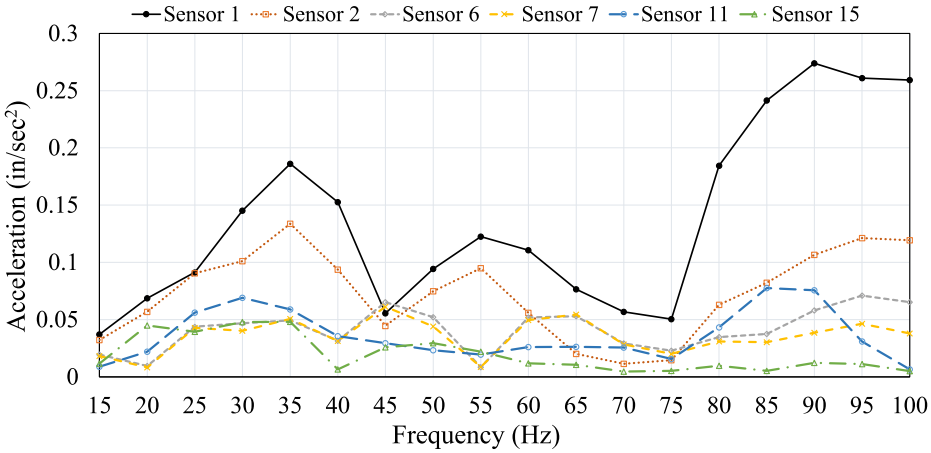


**Fig. 10.** Maximum Steady-State Response in Vertical Direction, Excitation distance 20ft for the test case P0S0. (Note: the number of sensors are as shown in Fig. 4).

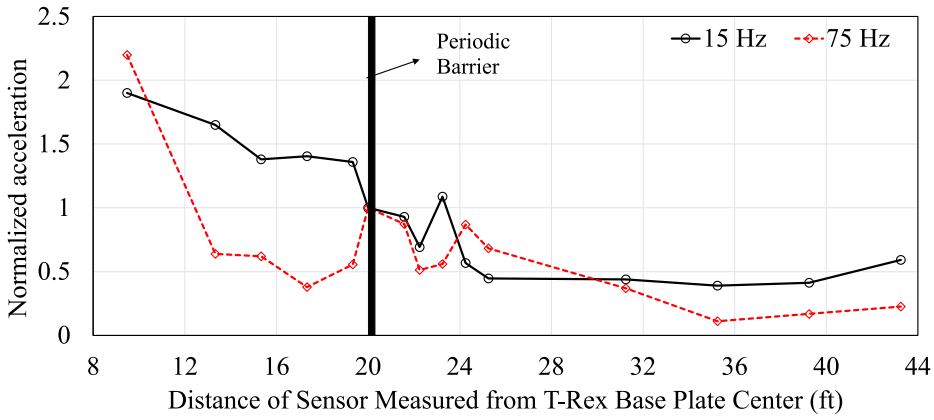


**Fig. 11.** Normalized Response in Vertical Direction for Excitation Distance 20ft (Black: 15 Hz, Red: 75 Hz). (For interpretation of the references to color in this figure legend, the reader is referred to the web version of this article.)

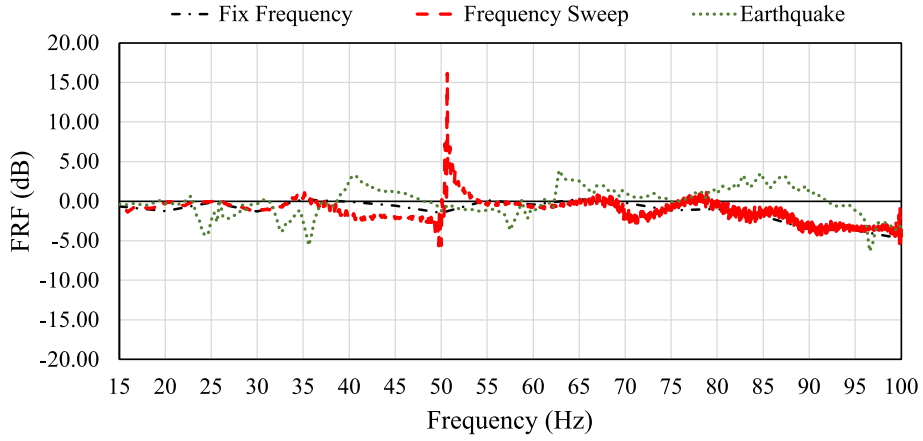


**Fig. 12.** FRF in Vertical Direction for Excitation Distance 20ft, Case P0S0.

The response of the ground surface after introducing the barrier (P0EL) is presented in Fig. 17.

The ground surface response of the P0S0 case is the benchmark case. Due to the stiffness and damping characteristics of soil, a small response is observed in the P0S0 case in Fig. 16 (a), Fig. 16 (b), and Fig. 16 (c) as the wave propagates away from the barrier, which is called geometric decay. With the presence of a long empty trench barrier, we expect the ground surface response to reduce further in addition to geometric decay. This is observed in Fig. 17 (a), Fig. 17 (b), and Fig. 17 (c). The frequency response function is calculated for both the P0S0 and P0EL cases to evaluate the frequency screening effectiveness of the barrier and to identify the frequency attenuation zone for the long-empty trench barrier. Fig. 18 shows the FRF of P0S0 and P0EL under frequency sweep excitation. The frequency attenuation zone is identified when the FRF is less than zero. When the FRF is greater than zero, the frequency magnification is identified. The result shows that the frequency attenuation zone for the long-empty trench barrier under the vertical direction of excitation, as shown in Fig. 18 (a), is found to be between 15 Hz and 38 Hz, 59 Hz-63 Hz, and 70 Hz-100 Hz, whereas the frequency magnification zone is found to be between 39 Hz – 58 Hz and 64 Hz – 69 Hz. Under the horizontal inline direction of excitation, the frequency attenuation zone is found to be between 15 Hz and 25 Hz, 27 Hz-42 Hz, and 50 Hz-100 Hz, as shown in Fig. 18 (b), whereas the frequency magnification zone is found to be between 25.1 Hz and 26.9 Hz and 43 Hz-49 Hz. Under the horizontal crossline excitation direction, frequency attenuation is observed to cover the full range of frequencies from 15 Hz to 100 Hz, as shown in Fig. 18 (c).

These results suggest that the presence of barrier induces response reduction in a particular range of frequencies which gives a way to isolate the seismic vibration by the periodic barrier.

### 4.3. *Single long periodic barrier (P0BL)*

A single long periodic barrier of the length of 8 ft, depth of 5 ft, and width of 0.92 ft is located between sensors 6 and 7, as shown previously in sensor mapping Fig. 5. When fix-frequency harmonic excitations are applied at a distance of 20 ft in the three excitation directions, the ground surface response is recorded in all three directions by the sensors. The critical points for observation are sensors 6 and 7. The normalized response is obtained by dividing the response of sensors 6 to 15 by sensor 6, which is the nearest sensor before the single long periodic barrier. When 15 Hz and 75 Hz harmonic excitations are applied at a distance of 20 ft from the barrier, the response reduction observations are discussed below. Fig. 19 (a)-(f) shows the normalized maximum response at sensor locations after the barrier under fix-frequency harmonic excitation at a distance of 20 ft. The black curve represents the benchmark case (P0S0), and the red curve represents the single long periodic barrier case (P0BL).

When a single long periodic barrier replaces the long empty trench, the response reduction is expected due to the screening effect of the periodic barrier. Even though the dimensions of the long-empty trench and the single long barrier are the same, the resulting response reduction is significantly different. When 15 Hz fix-frequency harmonic excitations are applied, an amplified response is observed under vertical and horizontal inline excitation directions, as shown in Fig. 19 (a) and Fig. 19 (b). The normalized maximum response of the P0BL case is larger

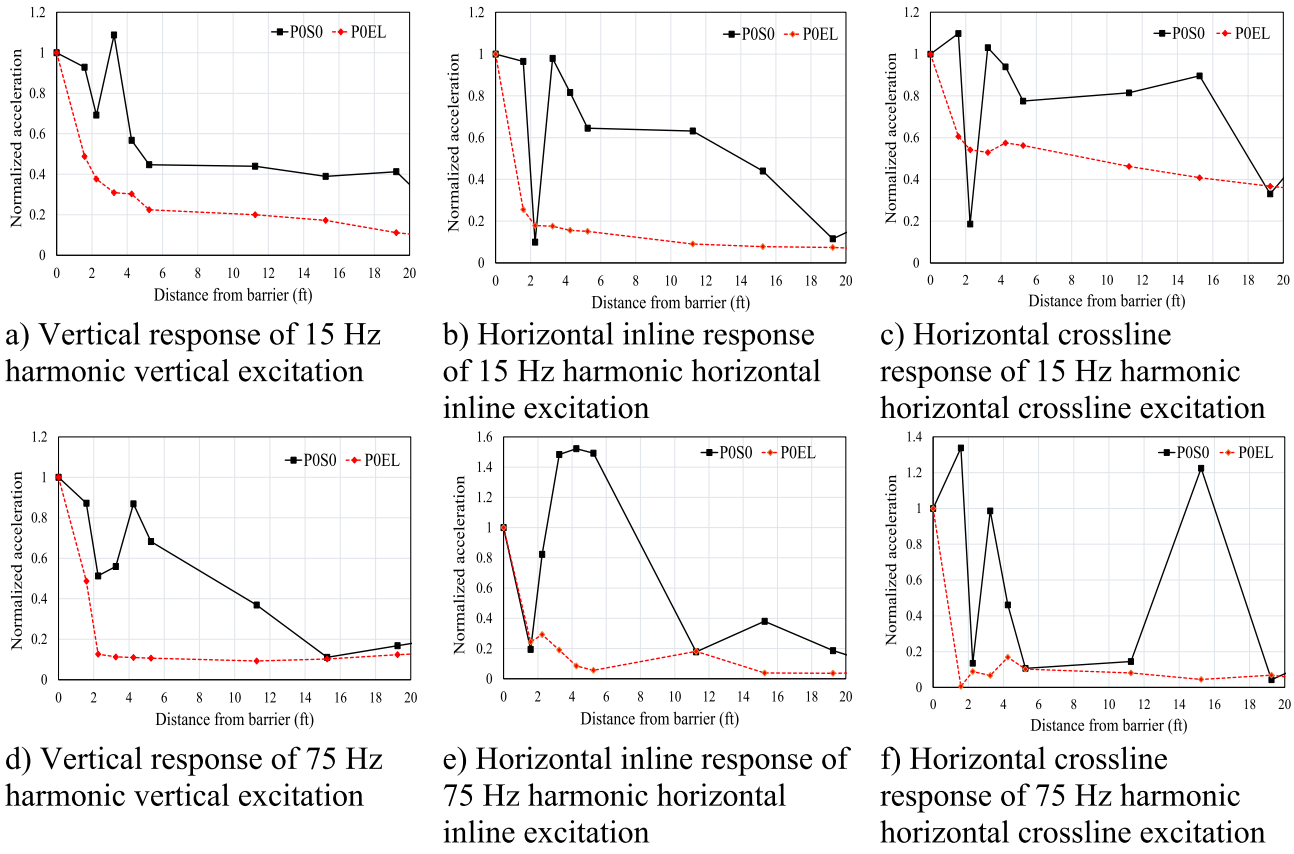


**Fig. 13.** Normalized Maximum Response of Sensors After the Long Empty Trench Under Fix frequency Harmonic Excitation at 20 ft Distance from barrier (Black: P0S0, Red: P0EL). (For interpretation of the references to color in this figure legend, the reader is referred to the web version of this article.)

than that of the P0S0 case. When 75 Hz fix-frequency harmonic excitations are applied, a response reduction is observed under vertical excitation, as shown in Fig. 19 (d). The normalized maximum response of the P0BL case is smaller than that of the P0S0 case. Therefore, the frequency screening performance of the barrier is strongly dependent on infilled material, excitation direction, and excitation frequency.

When the other two input signals, i.e., frequency sweep and earthquake excitation, are applied, the response is recorded by all the sensors. The two critical sensor locations are identified to analyze the isolation performance of the barrier. Sensor 6 is the nearest point before the barrier, and the response is considered as input to the barrier. Sensor 7 is the nearest point after the barrier, and the response is considered as output from the barrier. The results are represented in the frequency domain to evaluate the effect of exciting frequency on the barrier's performance. The ground surface response from the P0S0 case is represented in Fig. 20 (a)-(c), which show the characteristics of the test site. The response of the ground surface after introducing the single long barrier (P0BL) is represented in Fig. 21 (a)-(c).

Fig. 20 (a) shows that the ground surface response of the P0S0 case remains identical for the two critical sensor locations when the excitation is applied in the vertical direction. Under the horizontal inline and horizontal crossline excitations, the response remains similar within the frequency range of 15 Hz to 75 Hz, as shown in Fig. 20 (b) and Fig. 20 (c). After introducing the periodic barrier, the response reduction is significant at sensor 7. Under the vertical and horizontal crossline excitations, the decayed response shows the screening effectiveness of the periodic barrier, as shown in Fig. 21 (a) and Fig. 21 (c). Under the horizontal inline excitations, the amplified response is observed at the higher frequency range of 55 Hz to 95 Hz, as shown in Fig. 21 (b).

To demonstrate the screening effectiveness of the periodic barrier, the comparison of FRF is required with respect to the benchmark case. The FRF for both cases is calculated to identify the frequency attenuation zone for the single long periodic barrier. Fig. 22 (a)-(c) shows the FRF of P0S0 and P0BL under the frequency sweep excitation. Fig. 23 (a)-(c) shows the FRF of P0S0 and P0BL under earthquake excitation. The frequency attenuation zone is identified when the FRF is less than zero. When the FRF is greater than zero, the vibration magnification is identified. The black curve represents the P0S0 case, and the red curve represents the P0BL case.

Both the frequency sweep and the earthquake excitation provide similar results. The frequency attenuation zone for single long periodic barrier under the vertical direction of excitation is found to be between 21 Hz and 56 Hz and 71.5 Hz-100 Hz [Fig. 23 (a)], whereas the frequency magnification zone is found to be between 15 Hz and 20.5 Hz and 56.5 Hz-71 Hz. Under the horizontal inline direction of excitation, the frequency attenuation zone is found to be between 17.5 Hz and 29.5 Hz, and 43 Hz-56 Hz [Fig. 23 (b)], whereas the frequency magnification zone is found to be between 15 Hz and 17.5 Hz, 30 Hz-42.5 Hz, and 56.5 Hz-100 Hz. Under the horizontal crossline direction of excitation, the frequency attenuation zone is found to be between 15 Hz and 91.5 Hz, and 94.5 Hz-99.5 Hz [Fig. 23 (c)], whereas the frequency magnification zone is found to be between 91.5 Hz and 94.5 Hz. The theoretical frequency band gaps of the periodic barrier are stated in Section 3.1. The test results produce significantly similar frequency band gaps in the vertical and horizontal crossline excitation directions, whereas in the horizontal inline excitation direction, the results do not fit well with the theoretical frequency band gaps. This is due to the differences in assumptions, test conditions, and complex heterogeneous properties of soil. The theory of the metamaterial is built on the assumption that the material is infinitely large in its length and depth, and the boundary does not allow the vibration waves to bypass the periodic barrier.

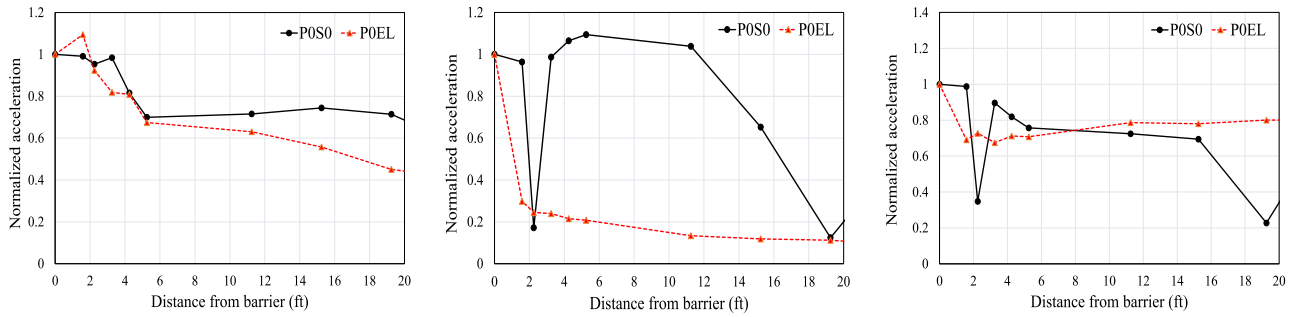


a) Vertical response of 15 Hz harmonic vertical excitation

b) Horizontal inline response of 15 Hz harmonic horizontal inline excitation

c) Horizontal crossline response of 15 Hz harmonic horizontal crossline excitation

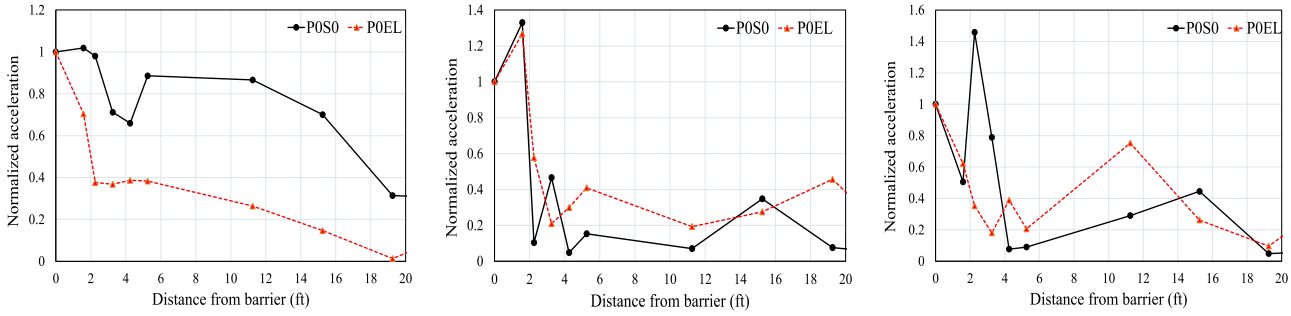


a) Vertical response of 75 Hz harmonic vertical excitation

b) Horizontal inline response of 75 Hz harmonic horizontal inline excitation

c) Horizontal crossline response of 75 Hz harmonic horizontal crossline excitation

**Fig. 14.** Normalized Maximum Response of Sensors After the Long Empty Trench Under Fix frequency Harmonic Excitation at 100 ft Distance (Black: P0S0, Red: P0EL). (For interpretation of the references to color in this figure legend, the reader is referred to the web version of this article.)

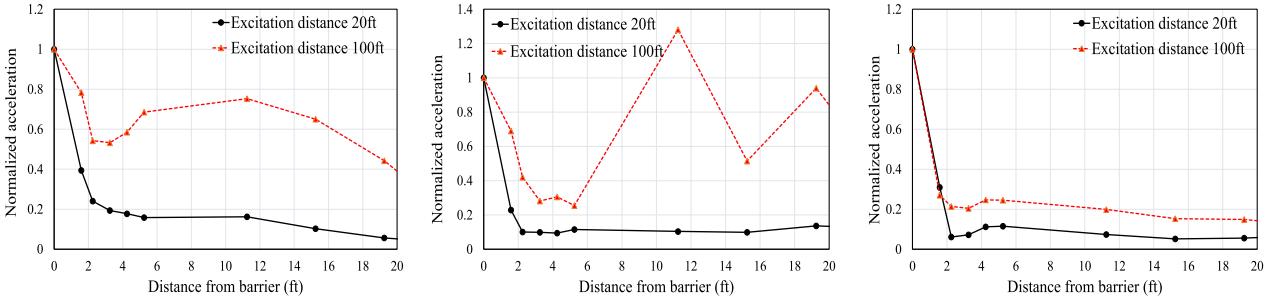


a) Vertical direction

b) Horizontal inline direction

c) Horizontal crossline direction

**Fig. 15.** Fix-frequency harmonic excitation at 30 Hz for P0EL case (Black: Excitation distance 20 ft, Red: Excitation distance 100 ft). (For interpretation of the references to color in this figure legend, the reader is referred to the web version of this article.)

### *4.4. One short thick barrier (P0B2T)*

In this special test case, one short thick periodic barrier of the length of 4 ft, depth of 5 ft, and width of 1.84 ft is located between sensors 6 and 7 by joining two single barriers, as shown previously in sensor mapping Fig. 6. Compared to the previous two cases, this is expected to give more vibration reduction since the barrier has two layers of polyurethane pads. The series of polyurethane pads will screen a wide range of frequencies, which provide a very wide frequency attenuation zone. The response is calculated in the direction the same as the excitation direction. When fix-frequency harmonic excitations are applied at a distance of 20 ft in the three directions, the ground surface response is recorded in the direction of excitation by all the sensors. The critical points for observation are sensors 6 and 7. The normalized response is obtained by dividing the response of sensors 6 to 15 by sensor 6 which is the nearest sensor before the short thick barrier. When 15 Hz and 75 Hz harmonic excitations are applied at a distance of 20 ft from the barrier, the ground surface response observations are discussed below. Fig. 24 (a)-(f) show the normalized maximum response at sensor locations after the barrier under fix-frequency harmonic excitations at a distance of 20 ft. The black curve represents the benchmark case (P0S0), and the red curve represents the one short thick periodic barrier case (P0B2T).

When the single short thick barrier is introduced, a response reduction is expected due to the reflection effect by the periodic barrier. When the fix-frequency harmonic excitations in the range from 15 Hz to 100 Hz with an increment of 5 Hz are applied, one low frequency and one high-frequency harmonic excitation response result are discussed below. When 15 Hz fix-frequency harmonic excitations are applied, an

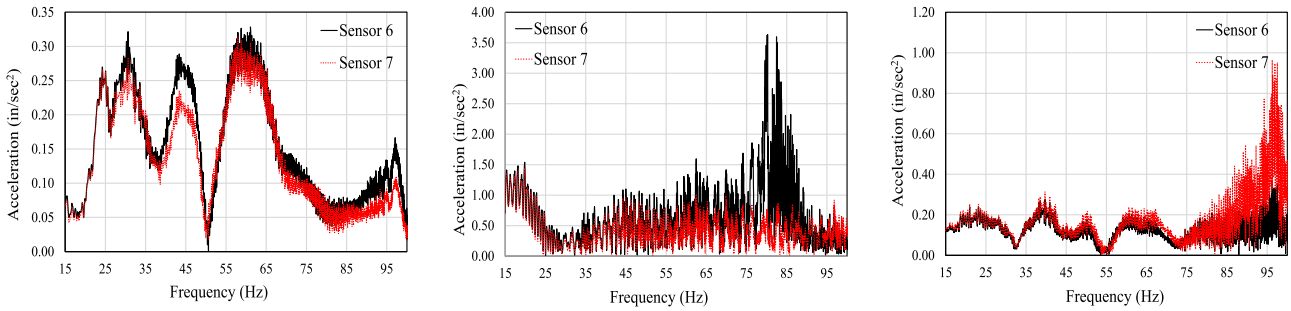


a) Vertical response of P0S0 under vertical excitation

b) Horizontal inline response of P0S0 under horizontal inline excitation

c) Horizontal crossline response of P0S0 under horizontal crossline excitation

**Fig. 16.** Ground Surface Response of P0S0 case under frequency sweeping excitation (Black: Sensor 6, Red: Sensor 7). (For interpretation of the references to color in this figure legend, the reader is referred to the web version of this article.)

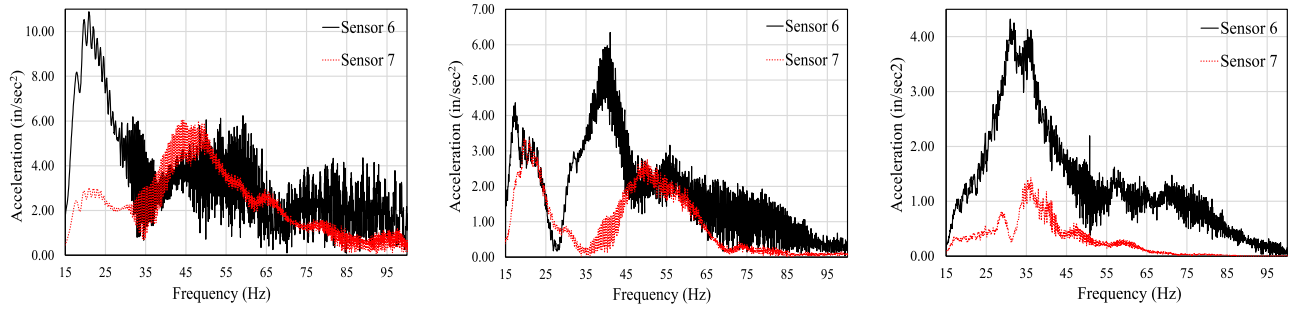


a) Vertical response of P0EL under vertical excitation

b) Horizontal inline response of P0EL under horizontal inline excitation

c) Horizontal crossline response of P0EL under horizontal crossline excitation

**Fig. 17.** Ground Surface Response of P0EL case under frequency sweeping excitation (Black: Sensor 6, Red: Sensor 7). (For interpretation of the references to color in this figure legend, the reader is referred to the web version of this article.)

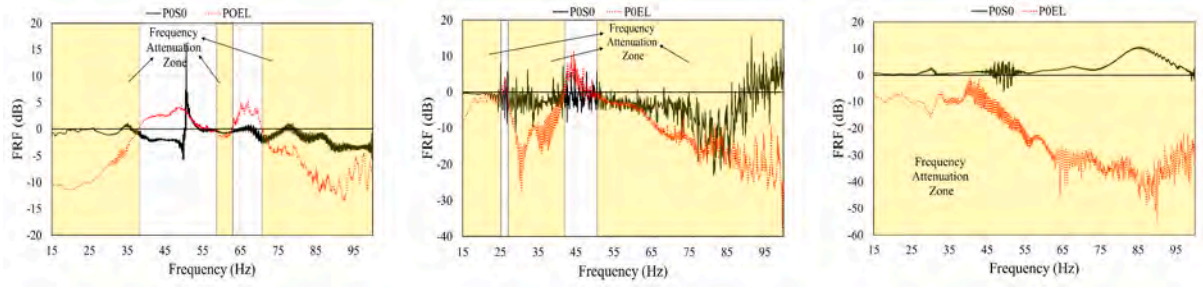


a) Vertical Response under vertical excitation

b) Horizontal inline response under horizontal inline excitation

c) Horizontal crossline response under horizontal crossline excitation

**Fig. 18.** FRF of P0S0 and P0EL under frequency sweep excitation (Black: P0S0 case, Red: P0EL case), the shaded area denotes the frequency attenuation zone of case P0EL. (For interpretation of the references to color in this figure legend, the reader is referred to the web version of this article.)

amplified response is observed under the vertical excitation direction [Fig. 24 (a)]. The normalized maximum response of the P0B2T case is larger than that of the P0S0 case. Whereas, when 75 Hz fix-frequency harmonic excitations are applied, decaying response reduction is observed [Fig. 24 (d)-(f)] as the wave propagates away from the barrier under all three excitation directions. The normalized maximum response of the P0B2T case is smaller than that of the P0S0 case.

When the other two input signals, i.e., frequency sweep and earthquake excitation are applied, the ground surface response is recorded by all the sensors. The two critical sensor locations are identified to analyze the isolation performance of the barrier. Sensor 6 is the nearest point before the barrier, and the response is considered as input to the barrier. Sensor 7 is the nearest point after the barrier, and the response is considered as output from the barrier. The results are represented in the frequency domain to evaluate the effect of exciting frequency on the barrier's performance. The ground surface response in the P0S0 case is the same as represented previously. The response of the ground surface after introducing the one short thick barrier (P0B2T) is represented in

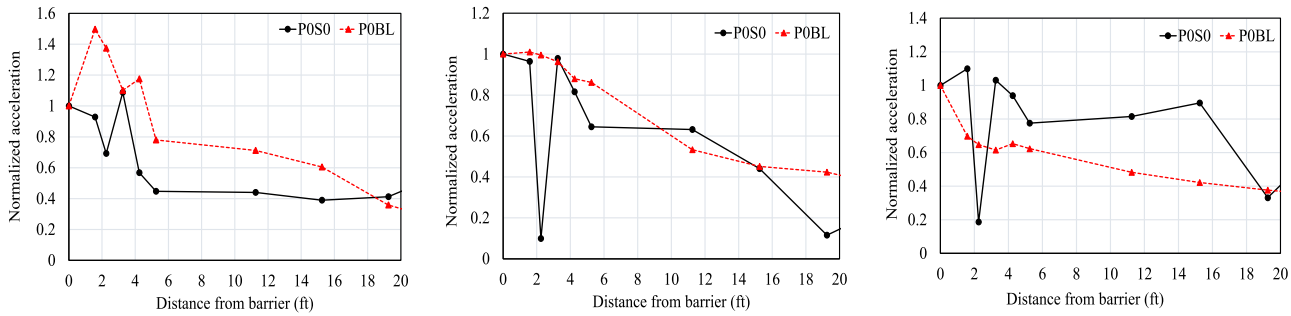


a) Vertical response of 15 Hz harmonic vertical excitation

b) Horizontal inline response of 15 Hz harmonic horizontal inline excitation

c) Horizontal crossline response of 15 Hz harmonic horizontal crossline excitation

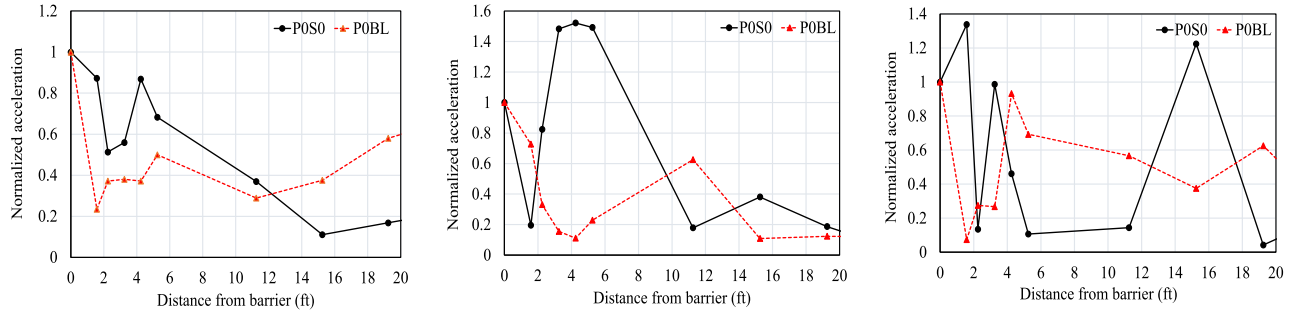


d) Vertical response of 75 Hz harmonic vertical excitation

e) Horizontal inline response of 75 Hz harmonic horizontal inline excitation

f) Horizontal crossline response of 75 Hz harmonic horizontal crossline excitation

**Fig. 19.** Normalized Maximum Response of Sensors After the Single Long Periodic Barrier Under Fix Frequency Harmonic Excitation at 20 ft Distance (Black: P0S0, Red: P0BL). (For interpretation of the references to color in this figure legend, the reader is referred to the web version of this article.)

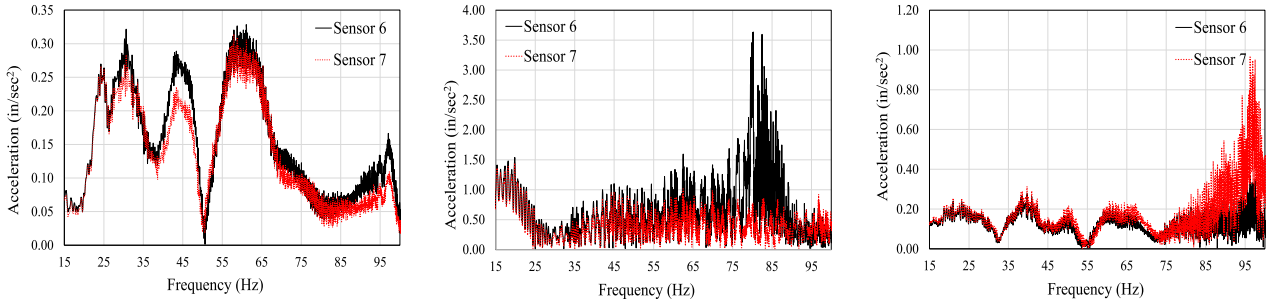


a) Vertical response of P0S0 under vertical excitation

b) Horizontal inline response of P0S0 under horizontal inline excitation

c) Horizontal crossline response of P0S0 under horizontal crossline excitation

**Fig. 20.** Ground Surface Response of P0S0 case under frequency sweeping excitation (Black: Sensor 6, Red: Sensor 7). (For interpretation of the references to color in this figure legend, the reader is referred to the web version of this article.)

Fig. 25 (a)-(c).

After introducing the short thick periodic barrier, as the wave propagates through the barrier, a significant response reduction is observed at sensor 7 under all three excitation directions. The decayed responses indicate the wave reflection effect of the periodic barrier.

To demonstrate the reflection effect of the periodic barrier, the comparison of FRF is required with respect to the benchmark case. The FRF for both cases is calculated to identify the vibration attenuation zone for the short thick periodic barrier. Fig. 26 (a)-(c) show the FRF of the P0S0 and P0B2T cases under frequency sweep excitations. Fig. 27 (a)-(c) show the FRF of the P0S0 and P0B2T cases under earthquake excitations. The vibration attenuation zone is identified when the FRF is less than zero. When the FRF is greater than zero, the frequency magnification is identified. The black curve represents the P0S0 case, and the red curve represents the P0B2T case.

Both the frequency sweep and the earthquake excitation give similar results. The vibration attenuation zone for the short thick periodic barrier under the vertical direction of excitation is found to be between 21 Hz and 31.5 Hz, and 36.5 Hz-100 Hz [Fig. 27 (a)], whereas the frequency magnification zone is found to be between 15 Hz and 20.5 Hz and 32 Hz-36 Hz. Under the horizontal inline direction of excitation, the vibration attenuation zone is found to be between 15 Hz and 100 Hz [Fig. 27 (b)]. Under the horizontal crossline direction of excitations, the vibration attenuation zone is found to be between 15 Hz and 44 Hz, and

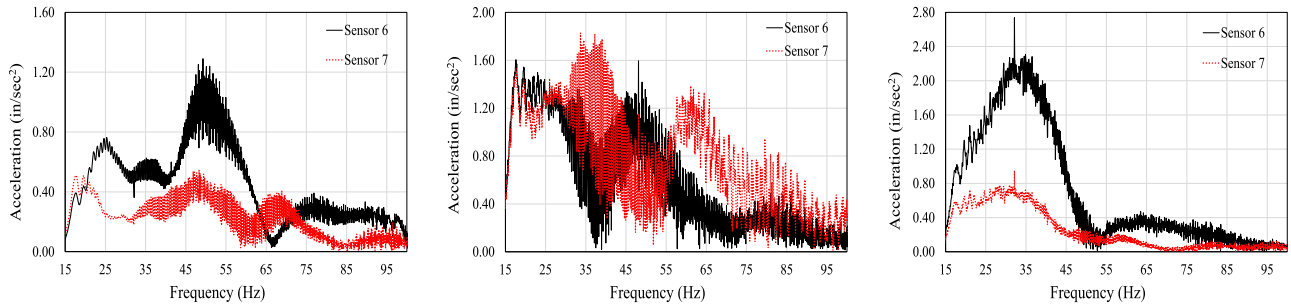


a) Vertical response of P0BL under vertical excitation

b) Horizontal inline response of P0BL under horizontal inline excitation

c) Horizontal crossline response of P0BL under horizontal crossline excitation

**Fig. 21.** Ground Surface Response of P0BL case under frequency sweeping excitation (Black: Sensor 6, Red: Sensor 7). (For interpretation of the references to color in this figure legend, the reader is referred to the web version of this article.)

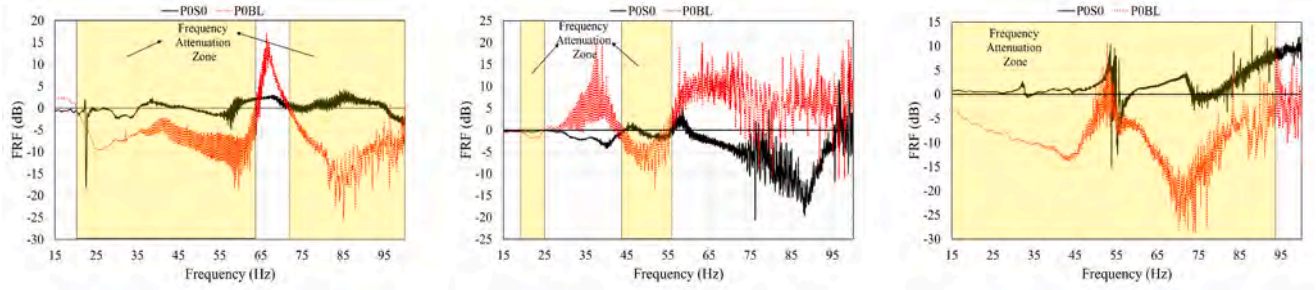


a) Vertical Response under vertical excitation

b) Horizontal inline response under horizontal inline excitation

c) Horizontal crossline response under horizontal crossline excitation

**Fig. 22.** FRF of P0S0 and P0BL cases under frequency sweep excitation (Black: P0S0 case, Red: P0BL case), the shaded area denotes the frequency attenuation zone of the case P0BL. (For interpretation of the references to color in this figure legend, the reader is referred to the web version of this article.)

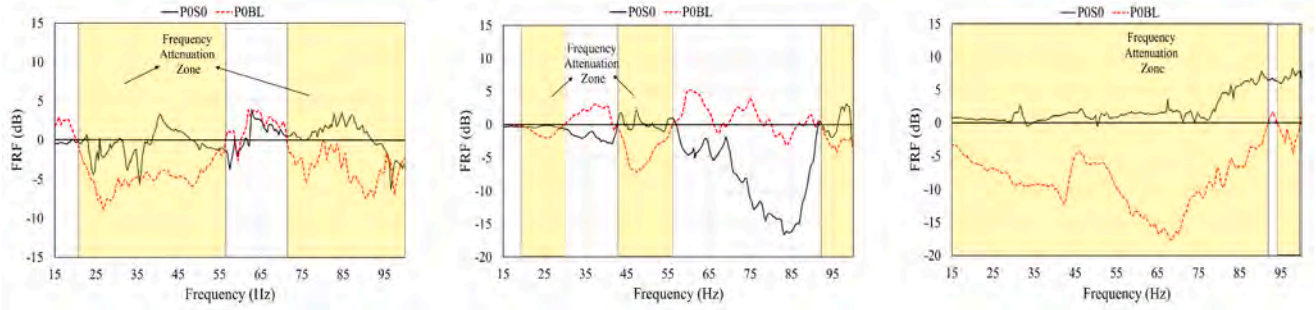


a) Vertical Response under vertical excitation

b) Horizontal inline response under horizontal inline excitation

c) Horizontal crossline response under horizontal crossline excitation

**Fig. 23.** FRF of P0S0 and P0BL cases under earthquake excitation (Black: P0S0 case, Red: P0BL case), the shaded area denotes the frequency attenuation zone of the case P0BL. (For interpretation of the references to color in this figure legend, the reader is referred to the web version of this article.)

50 Hz-100 Hz [Fig. 27 (c)], whereas the vibration magnification zone is found to be between 44.5 Hz and 49.5 Hz. The theoretical frequency band gaps of the periodic barrier are stated in Section 3.1. The test results indicate significantly similar frequency band gaps under the vertical and horizontal crossline excitation directions. On the contrary, the test results show that under the horizontal inline excitation direction, the vibration attenuation zone covers a wide range from 15 Hz to 100 Hz, whereas the theoretical frequency band gap lies between 45 Hz – 100 Hz. As expected, before the test, the series of periodic barriers screen a wide range of frequencies, making it a very reliable condition for vibration isolation.

## 5. Comparison of P0S0, P0EL, P0BL, and P0B2T test results.

The results from various test conditions are compared and discussed in this section. To evaluate the better performing test condition in

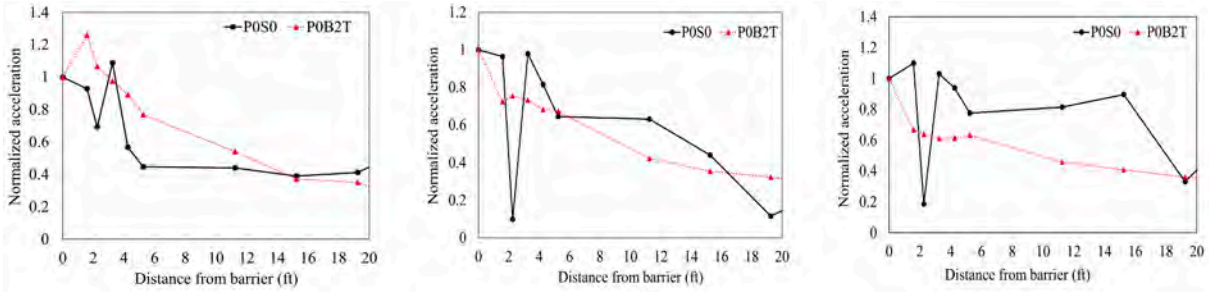


a) Vertical response of 15 Hz harmonic vertical excitation

b) Horizontal inline response of 15 Hz harmonic horizontal inline excitation

c) Horizontal crossline response of 15 Hz harmonic horizontal crossline excitation

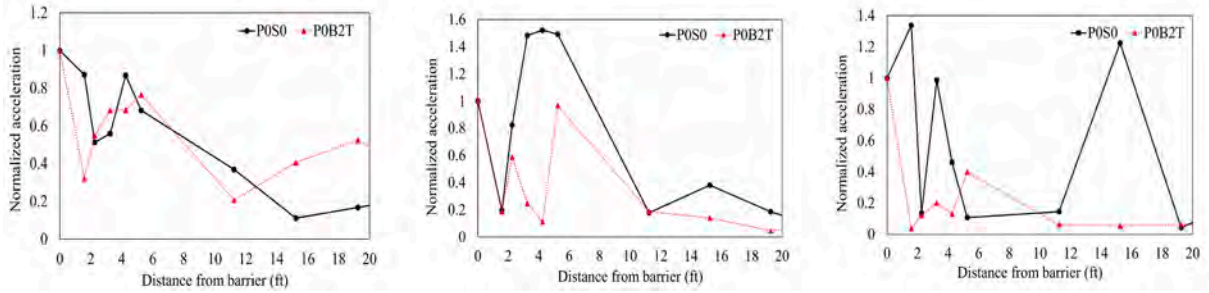


d) Vertical response of 75 Hz harmonic vertical excitation

e) Horizontal inline response of 75 Hz harmonic horizontal inline excitation

f) Horizontal crossline response of 75 Hz harmonic horizontal crossline excitation

**Fig. 24.** Normalized Maximum Response of Sensors After the One Short Thick Barrier Under Fix frequency Harmonic Excitation at 20 ft Distance (Black: P0S0, Red: P0B2T). (For interpretation of the references to color in this figure legend, the reader is referred to the web version of this article.)

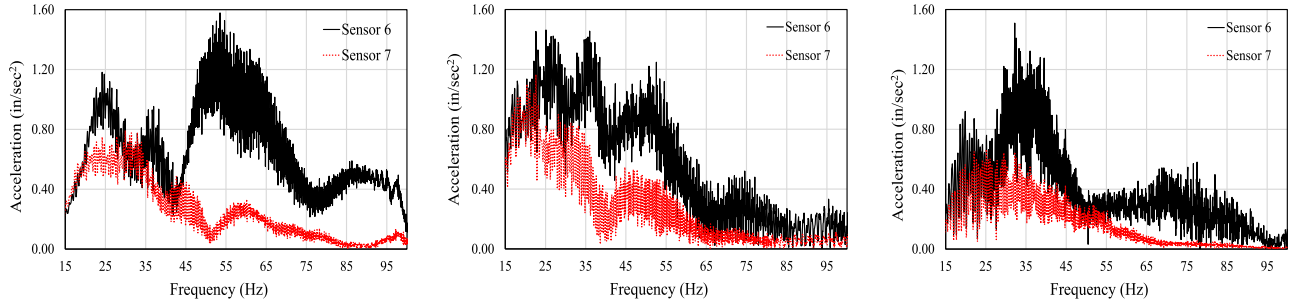


a) Vertical response of P0B2T under vertical excitation

b) Horizontal inline response of P0B2T under horizontal inline excitation

c) Horizontal crossline response of P0B2T under horizontal crossline excitation

**Fig. 25.** Ground Surface Response of P0B2T case under frequency sweeping excitation (Black: Sensor 6, Red: Sensor 7). (For interpretation of the references to color in this figure legend, the reader is referred to the web version of this article.)

isolation of vibration, all test results are represented in a single graph. The evaluation is quantified based on the Frequency Response Function (FRF). The FRF for each test condition is calculated as explained in Section 3.4. FRF is obtained by comparing the response in the front and at the back of the barrier. Fig. 28 (a)-(c) shows the FRFs of P0S0, P0EL, P0BL, and P0B2T cases under the fix frequency harmonic excitations in the vertical, horizontal inline, and horizontal crossline directions at a distance of 20 ft from the barrier.

As shown in Fig. 28 (a)-(c) and Fig. 29 (a)-(c), the responses vary with the distance of excitations from the barrier. As the distance of excitation source increases, the vibration energy of propagating wave decreases as it travels through the soil before reaching the barrier undergoing geometric decay due characteristic property of soil, i.e., density, stiffness, and damping. Hence the excitation distance is a key factor in vibration reduction performance of the barrier. Therefore, to evaluate the vibration reduction performance of various test conditions, the response results of excitations at a distance of 20 ft from the barrier are discussed below. Fig. 30 (a)-(c) show the FRFs under the fix-frequency harmonic, frequency sweep, and earthquake excitations in vertical direction at a distance of 20 ft from the barrier.

From Fig. 30 (a)-(c) it is evident that the test results are similar under all the three excitation inputs in the vertical direction. When the empty long trench is subjected to vertical excitations, minimum FRF can reach −14 dB, which is equal to 80 % response reduction. When a single long periodic barrier is subjected to vertical excitations, minimum FRF can reach −25 dB, which is equal to 94.4 % response reduction. When one

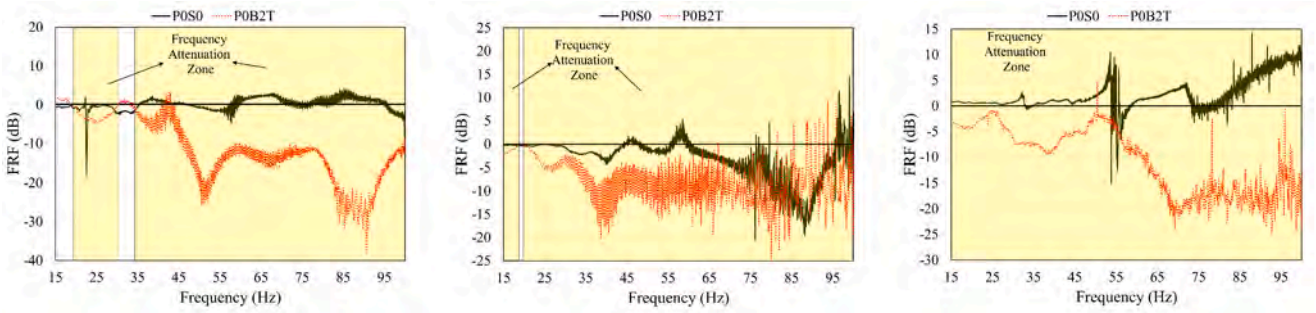


a) Vertical Response under vertical excitation

b) Horizontal inline response under horizontal inline excitation

c) Horizontal crossline response under horizontal crossline excitation

**Fig. 26.** FRF of P0S0 and P0B2T cases under frequency sweep excitation (Black: P0S0 case, Red: P0B2T case), the shaded area denotes the frequency attenuation zone of the case P0B2T. (For interpretation of the references to color in this figure legend, the reader is referred to the web version of this article.)

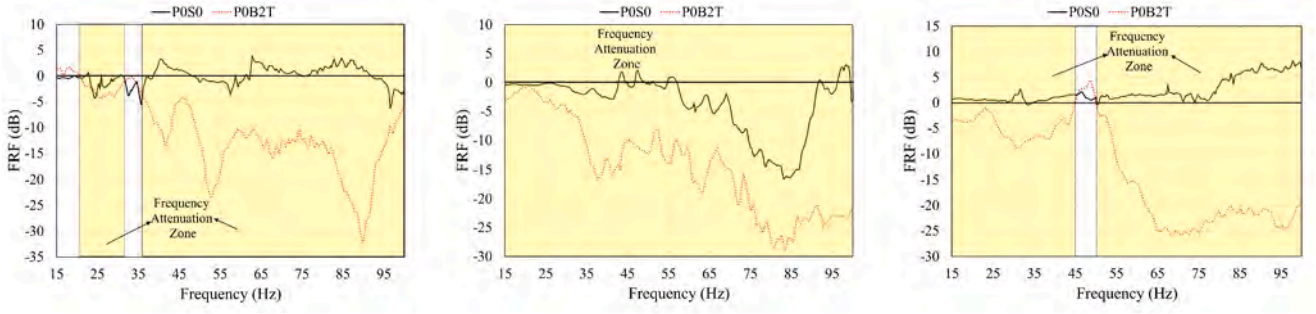


a) Vertical Response under vertical excitation

b) Horizontal inline response under horizontal inline excitation

c) Horizontal crossline response under horizontal crossline excitation

**Fig. 27.** FRF of P0S0 and P0B2T cases under earthquake excitation (Black: P0S0 case, Red: P0B2T case), the shaded area denotes the frequency attenuation zone of the case P0B2T. (For interpretation of the references to color in this figure legend, the reader is referred to the web version of this article.)

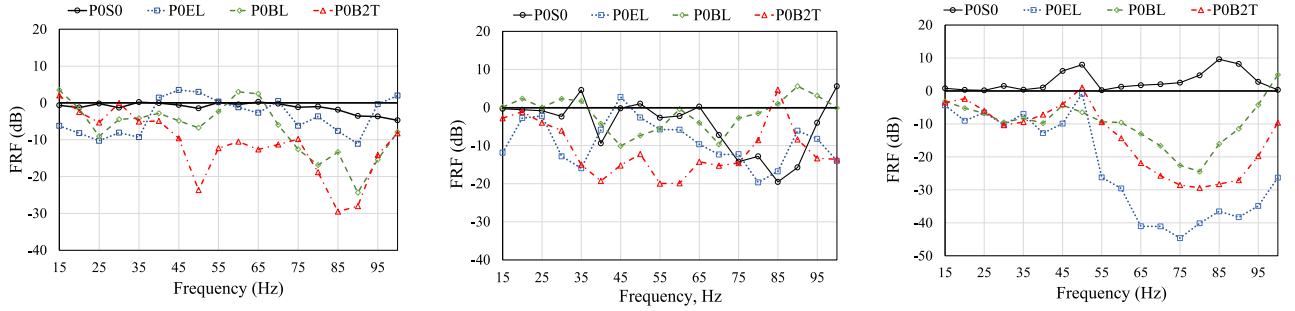


a) Vertical response under vertical excitation

b) Horizontal inline response under horizontal inline excitation

c) Horizontal crossline response under horizontal crossline excitation

**Fig. 28.** FRF under fix-frequency harmonic excitation at a distance of 20 ft from the barrier. (Black: P0S0, Blue: P0EL, Green: P0BL, Red: P0B2T). (For interpretation of the references to color in this figure legend, the reader is referred to the web version of this article.)

short thick periodic barrier is subjected to vertical excitation, the minimum FRF can reach −30 dB, which is equal to 96.8 % response reduction. The results indicate that the presence of a special case periodic barrier, P0B2T can isolate the vibration in the attenuation zones in the vertical direction of excitations to a greater extent.

To evaluate the vibration reduction performance of periodic barriers under horizontal inline and horizontal crossline excitation direction, the FRF is calculated for all the test cases and represented in a single graph. Fig. 31 (a)-(c) show the FRFs under fix-frequency harmonic, frequency sweep, and earthquake excitations in the horizontal inline direction at a distance of 20 ft from the barrier.

From Fig. 31 (a)-(c), it is evident that the test results are similar under all the three excitation inputs in the horizontal inline direction. To evaluate the performance of each test case, we need to calculate the

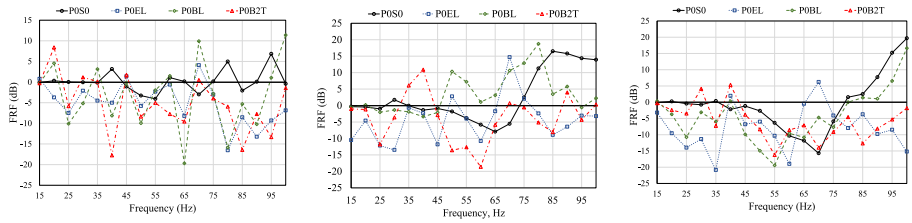


a) Vertical response under vertical excitation

b) Horizontal inline response under horizontal inline excitation

c) Horizontal crossline response under horizontal crossline excitation

**Fig. 29.** FRF under fix-frequency harmonic excitation at a distance of 100 ft from the barrier. (Black: P0S0, Blue: P0EL, Green: P0BL, Red: P0B2T). (For interpretation of the references to color in this figure legend, the reader is referred to the web version of this article.)

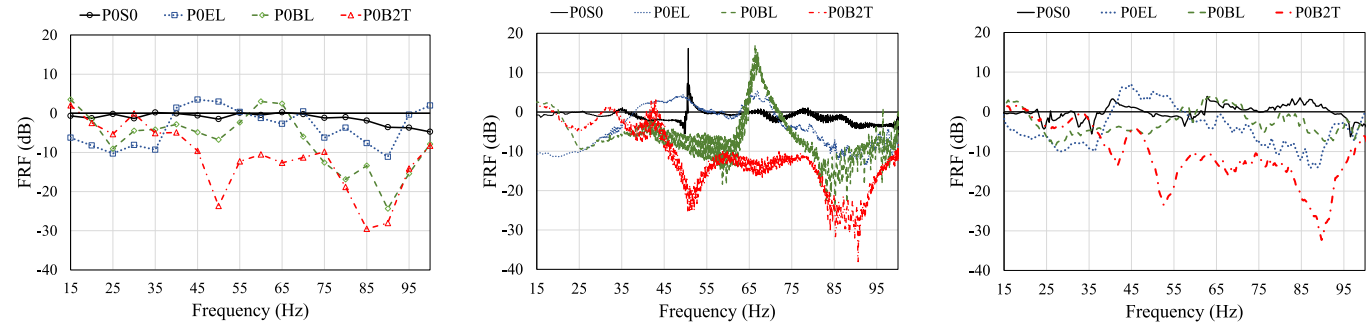


a) Fix-frequency harmonic b) Frequency sweep excitation c) Earthquake excitation

**Fig. 30.** FRF under Fix-frequency Harmonic, Frequency Sweep, and Earthquake Excitation in Vertical direction at a distance of 20 ft from barrier. (Black: P0S0, Blue: P0EL, Green: P0BL, Red: P0B2T). (For interpretation of the references to color in this figure legend, the reader is referred to the web version of this article.)

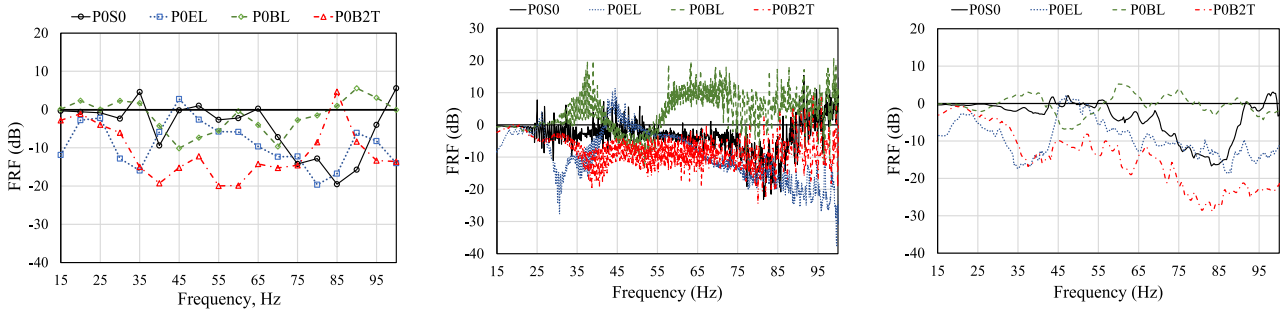


a) Fix-frequency harmonic b) Frequency sweep excitation c) Earthquake excitation

**Fig. 31.** FRF under Fix-frequency Harmonic, Frequency Sweep, and Earthquake Excitation in Horizontal inline direction at a distance of 20 ft from barrier. (Black: P0S0, Blue: P0EL, Green: P0BL, Red: P0B2T). (For interpretation of the references to color in this figure legend, the reader is referred to the web version of this article.)

percentage reduction in FRF (dB), as mentioned previously.

When an empty long trench is subjected to horizontal inline excitations, minimum FRF can reach −19 dB, which is equal to 88.8 % response reduction. When one single long periodic barrier is subjected to horizontal inline excitations, minimum FRF can reach −13.5 dB, which is equal to 79 % response reduction. When one short thick periodic barrier is subjected to horizontal inline excitations, minimum FRF can reach −28 dB, which is equal to 96 % response reduction. The results indicate that the presence of a special case periodic barrier, P0B2T can isolate the vibration in the attenuation zones in the horizontal inline direction of excitations to a greater extent. Whereas the single long barrier could not mitigate the vibration to the extent as provided by other cases.

To evaluate the vibration reduction performance of periodic barrier under both the horizontal inline and horizontal crossline excitation directions, the FRFs are calculated for all the test cases and represented in a single graph. Fig. 32(a)-(c) shows the FRFs under fix-frequency harmonic, frequency sweep, and earthquake excitations in horizontal inline direction at a distance of 20 ft from the barrier.

From Fig. 32 (a)-(c), it is evident that the test results are similar under all the three excitation inputs in the horizontal crossline direction. To evaluate the performance of each test case, we need to calculate the percentage reduction in FRF (dB), as mentioned previously.

When an empty long trench is subjected to horizontal crossline excitations, minimum FRF can reach −35 dB, which is equal to 98.2 % response reduction. When one single long periodic barrier is subjected to horizontal crossline excitations, minimum FRF can reach −24 dB, which is equal to 93.7 % response reduction. When one short thick periodic barrier is subjected to horizontal crossline excitation, minimum FRF can reach −29 dB, which is equal to 96.5 % response reduction. The results indicate that the presence of periodic barrier can mitigate the vibration in the attenuation zones in the horizontal crossline direction of

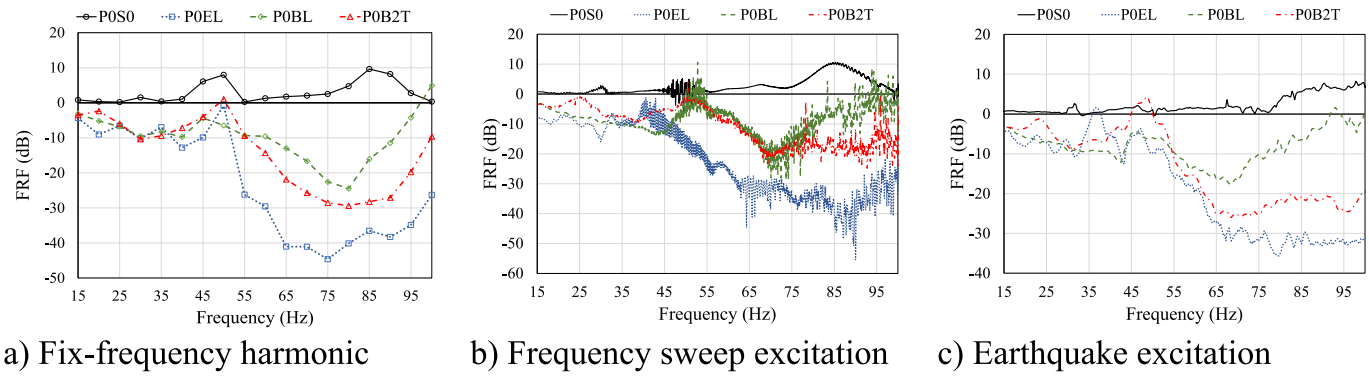


**Fig. 32.** FRF under Fix-frequency Harmonic, Frequency Sweep, and Earthquake Excitation in Horizontal crossline direction at a distance of 20 ft from barrier. (Black: P0S0, Blue: P0EL, Green: P0BL, Red: P0B2T,). (For interpretation of the references to color in this figure legend, the reader is referred to the web version of this article.)

excitations to a greater extent. Table 2 shows the response reduction for different test cases under different directions of excitation. The vibration reduction significantly depends on the type of infilled material, excitation direction, and excitation distance.

## 6. Conclusions

The seismic vibration isolation by a periodic barrier and an empty trench is studied through a series of large-scale field experiments. The trench-type wave barrier with various infilled material conditions is tested to evaluate the vibration isolation performance. Different excitation inputs like fix-frequency harmonic, frequency sweep and earthquake excitations are applied in various directions. From the results, the following conclusions can be drawn.

1. The similar results between the fix-frequency harmonic, frequency sweep, and earthquake excitations validates that signal generated by shaker can preserve the characteristics of the input signal and the test procedure is reliable for evaluating the vibration isolation performance of the periodic barrier.
2. The vibration isolation performance is not only dependent on infilled material and geometric property but also the excitation distance. As the distance of the excitation source from the periodic barrier increases, the vibration isolation performance reduces because the incoming wave propagates through the soil before reaching the barrier. Most of the energy associated with the incoming wave is absorbed by soil due to the characteristic properties of soil, such as density, stiffness, and Young's modulus, and it undergoes geometric decay.
3. The vibration isolation performance of the periodic barrier significantly depends on the excitation direction. A wide range of frequency band gaps can be seen in vertical and horizontal crossline directions of excitation, than in horizontal inline excitation directions. This indicates the better vibration isolation performance of periodic barrier for transverse and longitudinal waves, as concluded by previous researchers.
4. The use of a direct method to calculate the FRF is dependable for identifying the attenuation zones of the periodic barrier since it uses the nearest sensor before and after the barrier and it provides way to evaluate the local effect of periodic barrier in vibration isolation.
5. The test results shows that the empty trench does not necessarily outperform the periodic barrier. Under certain excitation frequencies and excitation directions, the periodic barrier works better than the empty trench particular for Rayleigh waves, 94.4 % and 96.8 % vibration reduction is observed in P0BL and P0B2T cases respectively when compared to only 80 % reduction for P0EL case. Hence the periodic barrier can be installed as a wave barrier, which overcomes the disadvantages associated with an empty trench.
6. When the unit cell is repeated to form short thick barrier, the vibration reduction can become more significant. The vibration reduces by 96.8 % under vertical, 96 % under horizontal inline, and 96.4 % under horizontal crossline excitation directions. This shows the effect of the number of barriers on vibration isolation.
7. The discrepancy between the attenuation zones identified through the field test and the theoretical frequency band gaps are found to be associated with the inclusion of the soil, i.e., the heterogeneous property of soil and characteristic properties of soil such as density, stiffness, and Young's modulus at the testing site.
8. When the frequency of incoming vibration falls within the attenuation zone associated with the periodic barrier, the metamaterial periodic barrier can isolate the vibration by reflecting them hence protecting the structure from seismic vibrations.

**Table 2**
Response reduction for different test cases.

| Excitation direction | Response reduction (dB) | | |
|---|---|---|---|
| | P0EL | P0BL | P0B2T |
| Vertical | 80 % | 94.4 % | 96.8 % |
| Horizontal inline | 88.8 % | 79 % | 96 % |
| Horizontal crossline | 98.2 % | 93.7 % | 96.5 % |

Data availability statement.

All the field experiment data that support the findings of this study are published in Designsafe [40] and can be accessed at https://doi.org/10.17603/ds2-c7wn-kj59.

## CRediT authorship contribution statement

**Nagesh H. Ramaswamy:** Methodology, Visualization, Data curation, Investigation. **Bhagirath Joshi:** Investigation, Visualization, Data curation. **Jiaji Wang:** Writing – original draft, Writing – review & editing, Methodology, Formal analysis, Visualization. **Xiaoliang Li:** Investigation, Visualization, Data curation. **F.Y. Menq:** Writing – review & editing, Data curation, Resources. **Xiaonan Shan:** Writing – review & editing, Validation, Supervision. **Kalyana Babu Nakshatrala:** Writing – review & editing, Validation, Supervision. **K.H. Stokoe:** Resources, Supervision, Project administration, Funding acquisition. **Y.L. Mo:** Writing – review & editing, Resources, Supervision, Project administration, Funding acquisition.

## Declaration of Competing Interest

The authors declare that they have no known competing financial interests or personal relationships that could have appeared to influence the work reported in this paper.

## Data availability

Data will be made available on request.

## Acknowledgments

This research is financially supported by the National Science Foundation (NSF) for Awards 1761659 and 1761597. We acknowledged the use of the facilities and instruments provided by NHERI@UTexas (CMMI-2037900 and CMMI-1520808), and authors would like to express the gratitude toward NHERI@UTexas for the execution of the experimental program. For the computational studies conducted in this research, authors acknowledge the use of Carya cluster, Sabine cluster and Opuntia cluster, provided by the Core Facility for Advanced Computing and Data Science at the University of Houston. Special thanks to Dr. Kevin Anderson at Austin Water - Center for Environmental Research for the access to the Hornsby Bend Biosolids Management Plant test site.

## References

[1] Witarto W, Wang SJ, Nie X, Mo YL, Shi Z, Tang Y, et al. Analysis and design of one-dimensional periodic foundations for seismic base isolation of structures. Int J Eng Res Appl 2016;6(1):05–15.
[2] Hsuan Wen Huang. Periodic metamaterial-based seismic isolation barriers: Field studies and computational Modeling. University of Houston, Department of Civil and Environmental Engineering; 2020. PhD dissertation,.
[3] Zhao C, Zeng C, Witarto W, wen Huang H, Dai J, Mo YL. Isolation performance of a small modular reactor using 1D periodic foundation. Eng Struct 2021;244:112825.
[4] Witarto FNU, Mo Y-L, Tang Y, Kassawara R, Chang K-C. Periodic material-based seismic base isolators for small modular reactors. University of Houston, TX; 2018. Technical Report,.
[5] Cheng ZB, Shi ZF. Composite periodic foundation and its application for seismic isolation. Earthq Eng Struct Dyn 2018;47(4):925–44. https://doi.org/10.1002/eqe.2999.
[6] Cheng Z, Shi Z. Novel composite periodic structures with attenuation zones. Eng Struct 2013;56:1271–82. https://doi.org/10.1016/j.engstruct.2013.07.003.
[7] Woods RD. Screening of surface waves in soils. J Soil Mech Foundat Div 1968;94:951–80.
[8] Saikia A. Numerical study on screening of surface waves using a pair of softer backfilled trenches. Soil Dyn Earthq Eng 2014;65:206–13. https://doi.org/10.1016/j.soildyn.2014.05.012.
[9] Al-Hussaini TM, Ahmad S. Design of wave barriers for reduction of horizontal ground vibration. J Geotech Eng 1991;117(4):616–36.
[10] Alzawi A, Hesham El Naggar M. Full scale experimental study on vibration scattering using open and in-filled (GeoFoam) wave barriers. Soil Dyn Earthq Eng 2011;31(3):306–17. https://doi.org/10.1016/j.soildyn.2010.08.010.
[11] Leung KL, Vardoulakis IG, Beskos DE, Tassoulas JL. Vibration isolation by trenches in continuously nonhomogeneous soil by the BEM. Soil Dyn Earthq Eng 1991;10(3):172–9. https://doi.org/10.1016/0267-7261(91)90030-4.
[12] Coulier P, Hunt HEM. Experimental study of a stiff wave barrier in gelatine. Soil Dyn Earthq Eng 2014;66:459–63. https://doi.org/10.1016/j.soildyn.2014.08.011.
[13] Coulier P, Cuéllar V, Degrande G, Lombaert G. Experimental and numerical evaluation of the effectiveness of a stiff wave barrier in the soil. Soil Dyn Earthq Eng 2015;77:238–53. https://doi.org/10.1016/j.soildyn.2015.04.007.
[14] Çelebi E, Firat S, Beyhan G, Çankaya I, Vural I, Kirtel O. Field experiments on wave propagation and vibration isolation by using wave barriers. Soil Dyn Earthq Eng 2009;29(5):824–33. https://doi.org/10.1016/j.soildyn.2008.08.007.
[15] Pu X, Shi Z. Broadband surface wave attenuation in periodic trench barriers. J Sound Vib 2020;468:115130.
[16] Liao S, Sangrey DA. Use of piles as isolation barriers. J Geotech Eng Div 1978;104(9):1139–52. https://doi.org/10.1061/AJGEB6.0000684.
[17] Cai YQ, Ding GY, Xu CJ. Amplitude reduction of elastic waves by a row of piles in poroelastic soil. Comput Geotech 2009;36(3):463–73. https://doi.org/10.1016/j.compgeo.2008.08.015.
[18] Pu X, Shi Z. Periodic pile barriers for Rayleigh wave isolation in a poroelastic half-space. Soil Dyn Earthq Eng 121, 75–86, 2019, https://doi.org/10.1016/j.soildyn.2019.02.029.
[19] Pu X, Shi Z. Surface-wave attenuation by periodic pile barriers in layered soils. Constr Build Mater 2018;180:177–87. https://doi.org/10.1016/j.conbuildmat.2018.05.264.
[20] Huang J, Shi Z. Attenuation zones of periodic pile barriers and its application in vibration reduction for plane waves. J Sound Vib 2013;332(19):4423–39. https://doi.org/10.1016/j.jsv.2013.03.028.
[21] Torres M, Montero de Espinosa FR. Ultrasonic band gaps and negative refraction. Ultrasonics 2004;42:1–9. https://doi.org/10.1016/j.ultras.2004.01.041.
[22] Lucklum F, Vellekoop MJ. Realization of complex 3-D phononic crystals with wide complete acoustic band gaps. IEEE Trans Ultrason Ferroelectr Freq Control 2016;63(5):796–7. https://doi.org/10.1109/TUFFC.2016.2543527.
[23] Meseguer F, Holgado M, Caballero D, Benaches N, Sánchez-Dehesa J, López C, et al. Rayleigh-wave attenuation by a semi-infinite two-dimensional elastic-band-gap crystal. Phys Rev B 1999;59(19):12169–72. https://doi.org/10.1103/PhysRevB.59.12169.
[24] Zeng Y, Peng P, Du Q-J, Wang Y-S. A novel zero-frequency seismic metamaterial. 2019, preprint arXiv:1907.06446.
[25] Palermo A, Krödel S, Marzani A, Daraio C. Engineered metabarrier as shield from seismic surface waves. Sci Rep 2016;6. https://doi.org/10.1038/srep39356.
[26] Sanchez-Perez JV, Rubio C, Martinez-Sala R, Sanchez-Grandia R, Gomez V. Acoustic barriers based on periodic arrays of scatterers. Appl Phys Lett 2002;81(27):5240–2.
[27] Kushwaha MS, Halevi P, Dobrzynski L, Djafari-Rouhani B. Acoustic band structure of periodic elastic composites. Phys Rev Lett 1993;71(13):2022–5. https://doi.org/10.1103/PhysRevLett.71.2022.
[28] Yan Y, Laskar A, Cheng Z, Menq F, Tang Y, Mo YL, et al. Seismic isolation of two-dimensional periodic foundations. J Appl Phys 2014;116(4):044908. https://doi.org/10.1063/1.4891837.
[29] Huang HW, Wang J, Zhao C, Mo YL. Two-dimensional finite-element simulation of periodic barriers. J Eng Mech 2021;147(2). https://doi.org/10.1061/(asce)em.1943-7889.0001891.
[30] Zhao C, Zeng C, Huang H, Dai J, Bai W, Wang J, et al. Preliminary study on the periodic base isolation effectiveness and experimental validation. Eng Struct 2021;226:111364.
[31] Liu Z, Zhang X, Mao Y, Zhu YY, Yang Z, Chan CT, et al. Locally resonant sonic materials. Science 2000;289(5485):1734–6. https://doi.org/10.1126/science.289.5485.1734.
[32] Xiang HJ, Shi ZF, Wang SJ, Mo YL. Periodic materials-based vibration attenuation in layered foundations: experimental validation. Smart Mater Struct 2012;21(11):112003.
[33] Witarto W, Nakshatrala KB, Mo Y-L. Global sensitivity analysis of frequency band gaps in one-dimensional phononic crystals. Mech Mater 2019;134:38–53. https://doi.org/10.1016/j.mechmat.2019.04.005.
[34] Huang HW, Zhang B, Wang J, Menq F-Y, Nakshatrala KB, Mo YL, et al. Experimental study on wave isolation performance of periodic barriers. Soil Dyn Earthq Eng 2021;144:106602.
[35] Wang J, Huang HW, Zhang B, Menq F-Y, Nakshatrala KB, Mo YL, et al. Active isolation tests of metamaterial-based barriers and foundation. Eng Struct 2022;260:114253. https://doi.org/10.1016/j.engstruct.2022.114253.
[36] Zhang B, Huang HW, Menq F, Wang J, Nakshatrala KB, Stokoe KH, et al. Field experimental investigation on broadband vibration mitigation using metamaterial-based barrier-foundation system. Soil Dyn Earthq Eng 2022;155:107167.
[37] Stokoe K, Cox B, Clayton P, Menq F. NHERI@UTEXAS experimental facility with Large-scale mobile shakers for natural-hazards field studies. In: 2020. Frontiers in Built Environment, https://doi.org/10.3389/fbuil.2020.575973.
[38] Charles K. Introduction to Solid State Physics. 8th ed. Wiley; 2004.
[39] Witarto W, Wang SJ, Yang CY, Nie X, Mo YL, Chang KC, et al. Seismic isolation of small modular reactors using metamaterials. AIP Adv 2018;8(4):045307.
[40] Mo Y, Stokoe K, Menq F, Wang J, Zhang B, Huang H, Ramaswamy N. Seismic Isolation of Embedded Foundations Using Periodic Meta-material Barriers to Create Resilient Structures. Designsafe-CI, 2022. https://doi.org/10.17603/ds2-c7wn-kj59.
[41] Han L, Zhang Y, Ni ZQ, Zhang ZM, Jiang LH. A modified transfer matrix method for the study of the bending vibration band structure in phononic crystal Euler beams. Physica B Condens Matter 2012;407(23):4579–83. https://doi.org/10.1016/j.physb.2012.08.022.
[42] Chen AL, Wang YS. Study on band gaps of elastic waves propagating in one-dimensional disordered phononic crystals. Physica B Condens Matter 2007;392(1–2):369–78. https://doi.org/10.1016/j.physb.2006.12.004.
[43] Sigalas MM, Economou EN. Elastic and acoustic wave band structure. J Sound Vib 1992;158(2):377–82.
[44] Tomoyuki Kurose, Kenji Tsuruta, Chieko Totsuji, Hiroo Totsuji. Fdtd simulations of acoustic waves in two-dimensional phononic crystals using parallel computer. Memoirs Fac Eng, Okayama University 43 (2009) 16-21.
[45] Hsieh P-F, Tsung-Tsong Wu, Sun J-H. Three-dimensional phononic band gap calculations using the FDTD method and a PC cluster system. IEEE Trans Ultrason Ferroelectr Freq Control 2006;53:148–58.